Bromine atom production and chain propagation during springtime Arctic ozone depletion events in Barrow, Alaska

Chelsea R. Thompson,[1,a,b] Paul B. Shepson,[1,2] Jin Liao,[3,c,d] L. Greg Huey,[3] Chris Cantrell[4,e], Frank Flocke[4], and John Orlando[4]

[1]Department of Chemistry, Purdue University, West Lafayette, IN, USA

[2]Department of Earth and Atmospheric Sciences and Purdue Climate Change Research Center, Purdue University, West Lafayette, IN, USA

[3]School of Earth and Atmospheric Sciences, Georgia Institute of Technology, Atlanta, GA, USA

[4]National Center for Atmospheric Research, Boulder, CO, USA

[a]now at: Cooperative Institute for Research in Environmental Sciences, University of Colorado Boulder, Boulder, CO, USA

[b]now at: Chemical Sciences Division, NOAA Earth System Research Laboratory, Boulder, CO, USA

[c]now at: Atmospheric Chemistry and Dynamics Laboratory, NASA Goddard Space Flight Center, Greenbelt, MD, USA

[d]now at: Universities Space Research Association, Columbia, MD, USA

[e]now at: Department of Atmospheric and Ocean Sciences, University of Colorado Boulder, Boulder, CO, USA

Correspondence to: C. R. Thompson (chelsea.thompson@noaa.gov)

Abstract. Ozone depletion events (ODEs) in the Arctic are primarily controlled by a bromine radical-catalyzed destruction mechanism that depends on the efficient production and recycling

of Br atoms. Numerous laboratory and modeling studies have suggested the importance of heterogeneous recycling of Br through HOBr reaction with bromide on saline surfaces. On the other hand, the gas-phase regeneration of bromine atoms through BrO-BrO radical reactions has been assumed to be an efficient, if not dominant, pathway for Br reformation and thus ozone destruction. Indeed, it has been estimated that the rate of ozone depletion is approximately equal to twice the rate of the BrO self-reaction. Here, we use a zero-dimensional, photochemical model, largely constrained to observations of stable atmospheric species from the 2009 OASIS campaign in Barrow, Alaska, to investigate gas-phase bromine radical propagation and recycling mechanisms of bromine atoms for a seven-day period during late March. This work is a continuation of that presented in Thompson et al. (2015) and utilizes the same model construct. Here, we use the gas-phase radical chain length as a metric for objectively quantifying the efficiency of gas-phase recycling of bromine atoms. The gas-phase bromine chain length is determined to be quite small, at <1.5, and highly dependent on ambient O_3 concentrations. Furthermore, we find that Br atom production from photolysis of Br_2 and BrCl, which is predominately emitted from snow and/or aerosol surfaces, can account for between 30 – 90% of total Br atom production. This analysis suggests that condensed phase production of bromine is at least as important as, and at times greater than, gas-phase recycling for the occurrence of Arctic ODEs. Therefore, the rate of the BrO self-reaction is not a sufficient estimate for the rate of O_3 depletion.

1 Introduction

The springtime depletion of boundary layer ozone in the Arctic has been the subject of intense research for several decades. Early observations revealed a strong correlation between

ozone depletion events (ODEs) and enhancements in filterable bromine (Barrie et al., 1988). This discovery led researchers to propose a mechanism for the bromine-catalyzed destruction of ozone.

$Br_2 + h\nu \rightarrow 2Br$ (R1)

$Br + O_3 \rightarrow BrO + O_2$ (R2)

$BrO + BrO \rightarrow Br_2 \text{ (or } Br + Br) + O_2$ (R3)

This reaction cycle requires an initial source of bromine atoms to the boundary layer. Laboratory and theoretical studies have suggested that Br_2 could be produced through oxidation of bromide present in salt-enriched snow, ice or aerosol surfaces by gas-phase ozone (Hirokawa et al., 1998; Oum et al., 1998b; Gladich et al., 2015).

$O_3 + 2Br^-_{(aq)} + 2H^+_{(aq)} \rightarrow\rightarrow Br_2 + O_2 + H_2O$ (R4)

Field observations by Pratt et al. (2013) using a controlled snow chamber experiment with natural tundra snow collected near Barrow, AK lend further evidence to this mechanism, and also suggest Br_2 production from OH produced photochemically within the snowpack. This mechanism was further explored in the modeling study of Toyota et al. (2014) that suggested an important role for this activation pathway in producing bromine within the snowpack interstitial air.

Once present in the gas-phase, bromine atoms can be regenerated through radical-radical reactions of BrO with XO (where X = Br, Cl, or I), NO, OH, or CH_3OO to propagate the chain reaction and continue the destruction cycle of ozone. If BrO photolyzes or reacts with NO, O_3 is regenerated, and there is a null cycle with respect to O_3. However, although O_3 is not destroyed, these two pathways represent efficient routes for Br atom propagation. Thus R3 serves to make R2 effective in destruction of O_3. At the same time, Br atoms could be recycled through

heterogeneous reactions of HOBr with bromide in the condensed phase to release Br_2 to the gas-phase via the now well-known "bromine explosion" mechanism (Vogt et al., 1996; Tang and McConnell, 1996; Fan and Jacob, 1992).

$$BrO + HO_2 \rightarrow HOBr + O_2 \quad \text{(R5)}$$

$$HOBr_{(g)} \rightarrow HOBr_{(aq)} \quad \text{(R6)}$$

$$HOBr_{(aq)} + Br^-_{(aq)} + H^+_{(aq)} \leftrightarrow Br_{2(aq)} + H_2O \quad \text{(R7)}$$

$$Br_{2(aq)} \rightarrow Br_{2(g)} \quad \text{(R8)}$$

Evidence for reaction sequence R5 – R8 has been provided through laboratory studies, which found that Br_2 was produced when frozen bromide solutions were exposed to gas-phase HOBr (Huff and Abbatt, 2002; Adams et al., 2002). This mechanism is believed to proceed rapidly to produce Br_2 so long as sufficient bromide is present in an accessible condensed phase. The efficiency of this heterogeneous recycling mechanism has also been found to have a dependence on the acidity of the surface, as was shown using natural environmental snow samples in Pratt et al. (2013) and investigated in the modeling studies of Toyota et al. (2011, 2014), in a manner that is consistent with the stoichiometry of Reaction R7.

To efficiently sustain the ozone destruction cycle to the point of near complete loss of boundary layer ozone ($[O_3] < 2$ ppb), bromine atoms must be continually recycled through some combination of the above mechanisms. The gas-phase reaction cycle described by Reactions R1 – R3 has generally been considered to be the dominant pathway for Br reformation following the initial activation of Br_2 from the surface (the mechanism for which is still not fully understood). Thus, it has been assumed that the rate of ozone destruction can be estimated as Equation 1 (see Equation 15 in Hausmann and Platt, 1994, Equation 3 in Le Bras and Platt, 1995, and Equation 7

in Zeng et al., 2006), or as Equation 2 if chlorine chemistry is considered through Reaction R9 (Equation IX in Platt and Janssen, 1995).

$$-\frac{d[O_3]}{dt} = 2 \cdot k_3 \cdot [BrO]^2 \quad (1)$$

$$-\frac{d[O_3]}{dt} = 2(k_3 \cdot [BrO]^2 + k_9 \cdot [BrO] \cdot [ClO]) \quad (2)$$

$$BrO + ClO \rightarrow Br + OClO \quad (R9)$$

However, these approximations assume that the ozone destruction rate is dominated by the BrO + XO reaction, which in turn necessitates efficient gas-phase recycling of Br; therefore, a relatively long bromine chain length would be required to account for observed rates of ozone destruction. It is, however, possible that Br atoms are generated mostly by Br_2 photolysis, followed by BrO termination, e.g. by R5, in which case a short gas-phase bromine radical chain length would be implied. The chain length for any process depends on the rates of the propagation relative to the production and destruction reactions (Kuo, 1986). It is important to note that, in our definition, the chain length refers to radical propagation reactions occurring solely in the gas phase, and is a quantity completely independent of any condensed phase chemistry. In the stratosphere, the Br/BrO catalytic cycle can have a chain length ranging from 10^2 to 10^4 (Lary, 1996). In the troposphere, there is significantly less solar radiation and many more available sinks; thus, radical chain lengths can be much shorter. For example, the chain length of the tropospheric HO_x cycle has been estimated to be ~ 4 – 5 (Ehhalt, 1999; Monks, 2005), increasing to 10 – 20 near the tropopause (Wennberg et al., 1998). The halogen radical chain lengths in the Arctic troposphere have so far not been determined, thus, it is difficult to evaluate whether Equations 1 and 2 are appropriate for estimating ozone depletion rates.

The importance of heterogeneous reactions for recycling reactive bromine has been demonstrated in the recent literature (see review by Abbatt et al., 2012). Modeling studies using

typical Arctic springtime conditions to simulate ODEs have concluded that ozone depletion cannot be sustained without considering the heterogeneous recycling of reactive bromine on snow or aerosol surfaces (e.g., Michalowski et al., 2000; Piot and Von Glasow, 2008; Liao et al., 2012; Toyota et al., 2014). Michalowski et al. (2000) determined that the rate of ozone depletion in their model was limited by the mass transfer rate of HOBr to the snowpack (effectively, the rate at which Br is recycled through the heterogeneous mechanism) and that the depletion of ozone is nearly completely shut down when snowpack interactions are removed. Piot and von Glasow (2008) simulated ozone depletion using the one-dimensional MISTRA model and concluded that major ODEs (defined as complete destruction within 4 days) could only be produced if recycling of deposited bromine on snow is included. Without heterogeneous recycling on the snowpack, the BrO_x termination steps and irreversible loss of HOBr and HBr to the surface prohibits the occurrence of an ODE. More recently, using HOBr observations from Barrow during OASIS, Liao et al. (2012b) found that a simple photochemical model over-predicted observed HOBr during higher wind events (> 6 m s^{-1}), ostensibly due to an under-predicted heterogeneous loss to aerosol in the model, and concluded that their field observations support the hypothesis of efficient recycling back to reactive bromine via this mechanism.

It it is evident that the reactions occurring on snow and aerosol surfaces are likely the initial source of halogen species to the polar boundary layer and that heterogeneous bromine recycling on these surfaces must be considered for HOBr and HBr (as well as $BrNO_2$ and $BrONO_2$ in higher NO_x environments). However, the relative importance of gas-phase recycling of bromine atoms is uncertain, even though is it often assumed that the ozone depletion rate can be estimated reasonably well by the catalytic gas-phase radical reaction rates. The goal of this work was to investigate gas-phase Br atom propagation in terms of the bromine chain length in

comparison to the production of Br atoms through photolysis of Br_2 and BrCl, which are predominantly produced directly from surface emissions and/or aerosol release. Here, we present results from our study using a zero-dimensional model constrained with time-varying measurements of molecular halogens, HOBr, O_3, CO, NO, NO_2, and VOCs from the 2009 Ocean-Atmosphere-Sea Ice-Snowpack (OASIS) campaign in Barrow, Alaska. This work builds on the analysis presented in Thompson et al. (2015) using the same model framework. By constraining our model with observations, we were able to conduct an in-depth study of the halogen atom recycling occurring under varying conditions that were observed during the campaign.

2 Experimental

2.1 Measurements and Site Description

The analysis presented herein utilizes observations conducted during the OASIS field campaign that occurred during the months of February through April of 2009 in Barrow, AK. The goal of the OASIS study was to investigate the chemical and physical processes occurring within the surface boundary layer during ozone and mercury depletion events in polar spring. This study resulted in the largest suite of simultaneous and co-located atmospheric measurements conducted in the Arctic near-surface atmosphere to date, and represents a unique opportunity for in-depth examination of a multitude of chemical interactions in this environment.

Atmospheric measurements were conducted from instrument trailers located near the Barrow Arctic Research Consortium (BARC) facility on the Naval Arctic Research Laboratory (NARL) campus. Winds arriving at the site are primarily northeasterly, from over the sea ice, and thus represent background conditions with influence from natural processes and snow-air

interactions. Winds occasionally shift to westerly, bringing local emissions from the town of Barrow to the site; however, these isolated events are easily identifiable by coincident enhancements in both NO_x and CO.

Measurements of molecular halogens, HOBr, NO, NO_2, O_3, CO, and VOCs were used to constrain the model employed in this analysis. Instrumental methods for these measurements have all been described elsewhere, thus, only a brief description is provided here. Inorganic halogen species (Br_2, Cl_2, BrO, and HOBr) were measured by chemical ionization mass spectrometry with I^- ion chemistry as described in Liao et al. (2011, 2012, 2014); O_3, NO, and NO_2 were measured by chemiluminscence (Ridley et al., 1992; Ryerson et al., 2000). CO was measured using a standard commercial CO analyzer (Thermo Scientific) with infrared absorption detection, and formaldehyde (HCHO) was measured at 1 Hz frequency using a tunable diode laser absorption spectrometer, as described in Fried et al. (1997) and Lancaster et al. (2000). A large suite of organic compounds was measured in situ by fast GC-MS (Apel et al. 2010) and via whole air canister samples with offline GC-MS (Russo et al., 2010).

2.2 Model Description

The model used for this study is a zero-dimensional box model developed using the commercial software FACSIMILE. A detailed description of the model can be found in Thompson et al. (2015). We will describe the model only briefly here.

Our model consists of 220 gas-phase reactions and 42 photolysis reactions, representing much of the known gas-phase chemistry occurring in the Arctic, including the important halogen, HO_x, NO_x and VOC chemistry associated with ozone depletions. The model also includes an inorganic iodine reaction scheme adapted from McFiggans et al. (2000, 2002), Calvert and

195 Lindberg (2004) and Saiz-Lopez et al. (2008). Although IO has not been unambiguously
196 measured in the High Arctic above the ~1.5 – 2 pptv detection limit of LP-DOAS (long-path
197 differential optical absorption spectroscopy), observed enhancements in filterable iodide and
198 total iodine suggest that iodine chemistry is active to some extent in this region (Sturges and
199 Barrie, 1988; Martinez et al., 1999; Mahajan et al., 2010; Hönninger, 2002). Recently, I_2 has
200 been detected at tens of pptv within the snowpack interstitial air near Barrow, AK and at ≤0.5
201 pptv in the near surface air by I^- CIMS, providing direct evidence supporting the presence of at
202 least low levels of iodine chemistry (Raso et al., 2016). In our previous study (Thompson et al.,
203 2015), we investigated the impact of two different hypothetical levels of iodine. Here, we
204 investigate only the "Low Iodine" scenario for certain calculations, in which a diurnally varying
205 I_2 flux is incorporated such that average daytime mixing ratios of IO remain near 1 pptv for the
206 majority of the simulation. These levels of IO are realistic given our current knowledge based on
207 the work of Hönninger (2002) and Raso et al. (2016).

208 All gas-phase rate constants used in this model were calculated for a temperature of 248
209 K, consistent with average daytime conditions in Barrow for the period simulated. Although
210 some gas-phase reactions can exhibit a significant temperature dependence, we chose not to
211 incorporate variable temperatures into our model. This is justified in this case because ambient
212 temperature in Barrow for the week of 25 March 2009 varied by less than 10 K between the
213 maximum and minimum recorded daily temperatures. The radical oxidation and radical-radical
214 reactions that are of primary importance here do not have a large temperature dependence
215 (Atkinson et al., 2006, 2007); for example, a variability of 10 K imposes an ~1% change on the
216 rate of ethane oxidation by Cl atoms and a <4% change on the rate of the BrO + BrO radical self-
217 reaction. Most radical-radical reactions have only a small negative-temperature dependence.

Furthermore, and as mentioned previously, the major non-radical chemical species driving the model are highly constrained to observations and are not allowed to freely evolve. Table 1 contains an abbreviated list of the reactions included in the model, showing only those reactions that are central to the production, propagation, and termination of bromine radical chemistry, which is the focus of this study. A complete list of reactions can be found in Thompson et al. (2015).

The model is configured to simulate 7 days during late March, 25 through 31 March, that include a period of depleting ozone, a full ozone depletion ($[O_3] < 2$ ppbv) lasting for ~ 3 days, and recovery. The O_3 time-series for this period is shown in Figure 1A, along with radiation as a reference (all plots are in Alaska Standard Time). We constrain the model to observations for this time period by reading in time-varying data sets of O_3, C_2H_2, C_2H_4, C_2H_6, C_3H_8, C_3H_6, *n*-C_4H_{10}, *i*-C_4H_{10}, HCHO, CH_3CHO, CH_3COCH_3, methyl ethyl ketone (MEK), Cl_2, Br_2, HOBr, NO, NO_2, and CO at ten-minute time steps. All other gas-phase species are allowed to freely evolve. Surface fluxes (represented as volumetric fluxes) are used for HONO and I_2 and are scaled to $J(NO_2)$ as a proxy for radiation as both of these species are likely to be produced photochemically. Further discussion regarding HONO can be found in Thompson et al. (2015).

Photolysis rate constants (*J* coefficients) for many of the species included were calculated during OASIS using the Tropospheric Ultraviolent and Visible Radiation model from measurements of down-welling actinic flux conducted throughout the campaign (Shetter and Müller, 1999; Stephens et al., 2012). Estimates of J_{max} in the Arctic for OClO were taken from Pöhler et al. (2010), for HOCl from Lehrer et al. (2004), and for $CHBr_3$ from Papanastasiou et al. (2014). J_{max} values for the iodine compounds were calculated according the work of Calvert and Lindberg (2004), which also simulated conditions for late March in Barrow, Alaska. Time-

varying J coefficients for O_3 and NO_2 were read into the model at 10-minute time steps. All other photolysis reactions were scaled to $J(NO_2)$ in the modeling code using the maximum J coefficients (J_{max}) for 25 March (a clear-sky day) as a basis for scaling. For cloudy days, this method assumes that J coefficients for other photolytically-active species are attenuated in a manner that is proportional to $J(NO_2)$.

In the initial development of the model, heterogeneous reactions of halogen species occurring on aerosol and snowpack surfaces were included, as well as mass transfer and dry deposition for certain species using the method and mechanism of Michalowksi et al. (2000). This mechanism assumes aqueous phase kinetics for those reactions occurring within a uniformly distributed quasi-liquid layer (QLL), in a similar fashion as numerous other models (e.g., Piot and von Glasow, 2008; Thomas et al, 2011; Toyota et al., 2014). It was originally intended to utilize this multiphase chemistry to produce halogen radical precursors. However, the heterogeneous production mechanisms could not reproduce observed Br_2 or Cl_2 from OASIS. This reflects the complex but not fully understood condensed phase chemistry and physics that leads to production of Br_2 (and Cl_2) (Abbatt et al., 2012; Domine et al., 2013; Pratt et al., 2013). Additionally, the current knowledge of the physical properties of the QLL and the location of liquid-like surfaces on snow grains would seem to invalidate the aforementioned assumptions on which many of the current heterogeneous models are based (Domine et al., 2013), specifically that the chemistry occurs in a liquid-like environment on snow grains. Indeed, Cao et al. (2014), adopted a simplified heterogeneous chemistry mechanism in their modeling of Arctic ozone depletion, wherein they use the mass transfer of HOBr to the surface as the rate-limiting step in Br_2 production, citing the lack of suitable reaction mechanisms with which to properly simulate condensed phase chemistry on snow/ice. Admittedly, our model is also not able to capture these

264 complex heterogeneous processes. However, as discussed thoroughly by Domine et al. (2013),
265 even our most complex state-of-the-art snow chemistry models are neither physically nor
266 chemically accurate, and rely upon a variety of adjustable parameters to produce reasonable
267 results, because of the lack of fundamental understanding of the actual phase and physical and
268 chemical environment in which the chemistry is occurring. It is thus clear that the kinetics of the
269 individual reactions in such a case cannot be reliably simulated.

270 In light of the limitations of all models of cryosphere photochemistry, a strength of this
271 study, and opportunity, rests with the fact that we have observations of key halogen species,
272 including Br_2, Cl_2, BrO, ClO, HOBr, as well as VOCs, NO_x, OH and HO_2. Therefore, to study
273 the gas phase recycling discussed in the Introduction, in this work Br_2 and Cl_2 concentrations
274 were fixed at the observed levels (see Thompson et al., 2015 for further discussion) and were not
275 produced via heterogeneous chemistry. During a period spanning a portion of 29 and 30 March,
276 Br_2 observations are not available due to instrument instability. Here, we have filled in the
277 missing portion of data with average daytime Br_2 values based on observations from 27 and 28
278 March and the morning data available for 29 March, and use average nighttime values for the
279 night of 29/30 March using the observations from the two adjacent nighttime periods. The filled-
280 in values for Br_2 result in reasonable agreement between modeled and observed BrO for this
281 period. In the analyses presented in Figures 3 and 5 – 10 we have indicated this period of missing
282 and filled-in Br_2 values with a shaded box. Due to the sparseness of BrCl observations during
283 OASIS, only daytime BrCl was used as produced in the model multiphase mechanism. While
284 we do not argue that the production mechanism for BrCl is accurate, the daytime simulated BrCl
285 mixing ratios of 0 – 10 pptv are in approximate agreement with the available data for the

286 campaign. In any case, according to our model, BrCl was not a significant source of either Br or
287 Cl atoms relative to Br_2 and Cl_2.

288 Though we do not use the heterogeneous chemistry module for any chemical production
289 (other than BrCl), deposition and mass transfer is a significant and critical sink for certain
290 species. Thus, we do make use of this aspect of the multiphase portion of the model, as described
291 below. The dry deposition velocity of O_3 to the snowpack is estimated at 0.05 $cm \cdot s^{-1}$, consistent
292 with previous measurements and modeling studies (Gong et al., 1997; Michalowski et al., 2000;
293 Helmig et al., 2007; Cavender et al., 2008), though it is recognized that there is large uncertainty
294 with this parameter from field observations (Helmig et al., 2007, 2012). Assuming a boundary
295 layer height of 300 m, this corresponds to a transfer coefficient, k_t, of 1.67×10^{-6} s^{-1}. Though we
296 have incorporated the deposition of O_3 in the model, the *gas-phase* mixing ratio of O_3 is
297 constrained to observations, which adjusts on 10-minute time steps. Dry deposition velocities for
298 the stable Arctic environment have not been determined for the halogen acids (HBr, HCl, HOBr,
299 HOCl, HOI), therefore we use the estimation method of Michalowski et al. (2000) and assume a
300 deposition velocity that is 10 times greater than for O_3, leading to a k_t of 1.67×10^{-5} s^{-1}. In most
301 model runs, we have chosen to constrain to HOBr observations (further described in Section 3.1),
302 and thus a similar situation exists as for O_3 mentioned above. We assume an equivalent k_t for the
303 oxidized nitrogen compounds (HNO_3, HO_2NO_2, HONO, N_2O_5, $BrNO_2$, and $BrONO_2$). The mass
304 transfer coefficient of atmospheric species to the particle phase is calculated as a first-order
305 process as described in Jacob (2000). The concentration of aerosol surface area used was 3.95 x
306 10^{-7} cm^2 cm^{-3} as calculated by Michalowski et al. (2000) from measurements made at Alert by
307 Staebler et al. (1994), with a maximum aerosol radius of r = 0.1 μm. These levels are also
308 consistent with observations of aerosol surface area at Barrow, which ranged between 9 x 10^{-8}

309 cm^2 cm^{-3} and 40 x 10^{-7} cm^2 cm^{-3} (Liao et al. 2012b). We recognize that this constant level of
310 aerosols imparts a constant loss rate in the model and does not take into account any variability
311 in the uptake strength. Because many of these species are lacking empirically-derived deposition
312 velocities (e.g, HOBr), there is necessarily large uncertainty in these values, and it is not possible
313 at this time to ascertain whether the uncertainty associated with the deposition velocity
314 estimation is greater or less than the uncertainty imposed by using a constant aerosol surface area.
315 Liao et al. (2012b) did use time-varying aerosol surface area from observations at Barrow,
316 however, they suggested that simple parameterization of deposition of HOBr to aerosols was
317 insufficient for accurately simulating HOBr (further discussion of HOBr is in Section 3.1). Given
318 the highly simplified nature of the surface deposition in our model, we do not attempt to
319 differentiate between aerosol uptake and deposition to the snow surface, and instead we lump
320 these two terms together under the "surface deposition" umbrella. However, while we mostly
321 constrain the model to observed HOBr, the comparison to simulated HOBr using these values is
322 instructive.
323
324 **3 Results and Discussion**
325 **3.1 Comparison of modeled and observed Br_2, BrO, HOBr, and HO_2**
326 This work focuses on the propagation and production mechanisms of Br atoms, and thus
327 it is critical that our model accurately captures BrO and Br_2 at mixing ratios that are consistent
328 with observations. Figures 1B and 1C show comparisons between modeled mixing ratios (black
329 trace) of Br_2 and BrO compared to the measured values during this time (red data) by chemical
330 ionization mass spectrometry (CIMS) (Liao et al., 2012b). Modeled BrO is presented as hourly
331 averages. In the model, Br_2 is fixed to time-varying observations, whereas BrO is produced

strictly through the gas-phase photochemical reactions. The model captures the overall temporal profile and magnitude of BrO throughout the period. It should be noted, however, that the uncertainty in the BrO measurements is large during ODEs as the observed values are very near the detection limit (LOD of ~2 pptv with uncertainty of -3/+1 pptv near the LOD).

Br_2 mixing ratios reach 2 – 12 pptv (Figure 1B) during the daytime. Given the short lifetime of Br_2 resulting from rapid photolysis, these daytime mixing ratios imply a large surface flux, that in turn produces the BrO mixing ratios observed. These Br_2 levels are consistent with previous Arctic measurements that observed daytime Br_2 up to 27 pptv (Foster et al., 2001) and agree well with the "uncorrected" Br_2 data reported in Liao et al. (2012a, 2012b) for this period. It has been suggested that daytime Br_2 greater than the CIMS instrumental detection limit (~1 pptv) is an artifact of HOBr conversion to Br_2 on the instrument using an aircraft inlet (Neuman et al., 2010), however, for the instrument configuration employed during OASIS, it is not clear how much, if any, of the Br_2 signal is a result of HOBr reactions on instrument surfaces.

An estimate of the effective mixing height of Br_2 can be calculated using the method of Guimbaud et al. (2002) and using an average measured diffusivity during OASIS of 1500 $cm^2\ s^{-1}$ (R. Staebler, personal communication, 2015). By assuming that photolysis is the dominant loss mechanism controlling the Br_2 mid-day lifetime in a stable boundary layer typical of Arctic conditions, the daytime effective mixing height is ~1.85 m. This also assumes that the snowpack is the primary source of Br_2 emissions, which is consistent with previous assumptions for the aldehydes (Sumner et al., 1999; Guimbaud et al., 2002) and is supported by direct empirical evidence of the tundra snowpack being a relatively strong source of Br_2 (Pratt et al., 2013). Enhanced Br_2 within the snowpack interstitial air has also been predicted from the modeling studies of Toyota et al. (2011, 2014). From this estimation, a significant fraction of the Br_2

present at the surface would remain at the height of the instrument inlet (~1 m) in the sunlit periods. If aerosols do represent a significant source of Br_2 as has been hypothesized, and inferred indirectly from bromide depletion in sea salt aerosols (Sander et al., 2003), then one would expect enhanced Br_2 to be present throughout the height of the boundary layer. In our highly constrained model, daytime Br_2 mixing ratios greater than 1 pptv are necessary to reproduce observed BrO, therefore, this modeling study suggests that Br_2 should indeed be present and above the instrument detection limit during the daytime. Br atoms are predicted at concentrations ranging from 1 x 10^7 to 3 x 10^9 molecules cm^{-3}. The hourly averaged model output for Br is shown in Figure 2D. No direct measurements of Br atoms are available with which to compare, though these values are within the range of estimates determined by Jobson et al. (1994) and Ariya et al. (1998).

In the case of HOBr, our model originally simulated this species based on the known gas-phase sources and sinks (including photolysis) and deposition/uptake to surfaces as described above. As shown in Thompson et al. (2015), and again in Figure 2A, given the observed Br_2 mixing ratios, the model greatly overestimated HOBr. Liao et al. (2012b) simulated inorganic bromine species from the OASIS campaign using a simple steady-state model and experienced that their model also overestimated the observed HOBr, with the overestimation becoming especially pronounced during periods of higher winds. They suggested a faster heterogeneous loss to aerosols or blowing snow that was not represented in their model, despite utilizing time-varying aerosol surface area from observations. For the majority of the results presented in this work, we chose to operate our model constrained to HOBr observations, as illustrated in Figure 2B. Figure 2C shows modeled HOBr obtained by adjusting the deposition to aerosols based on daily wind speeds (resulting in k_t values ranging from $1x10^{-2}$ to $1.5x10^{-4}$ s^{-1}), and tuned to

provide reasonable agreement with observations. This resulted in smaller deposition rates on 25 through 27 March when winds were calm, and higher deposition rates on 29 through 31 March when winds were up to 9 m/s. This method allowed us to calculate the importance of surface deposition of HOBr relative to photolysis as a sink for this compound, but the constrained version of the model was used for all other calculations, e.g. for the chain length calculations.

HO_2 is essential for the heterogeneous recycling of bromine (via Reactions R5 – R7). Therefore, it is important that our model provides a reasonable estimation of HO_2 for this analysis. In Figure 1E we show a comparison of simulated, hourly-averaged HO_2 (black trace) and observed HO_2 from OASIS for this period (red data), measured using a CIMS developed for peroxy radicals (Edwards et al., 2003). The range of daytime HO_2 mixing ratios is reproduced reasonably well. Simulated HO_2 is on the lower limit of observations for 25 and 29 March, and does not reach the maximum mixing ratios observed. The model also somewhat overpredicts HO_2 on 28 through 30 March; however, the model values are within the stated 25% - 100% range of uncertainty of the measurement.

3.2 Chain length

The ozone destruction cycle as described in Reactions R1 – R3 is a chain reaction mechanism catalyzed by BrO_x. The effectiveness of a catalytic cycle can be quantified by considering the chain length, that is, the number of free radical propagation cycles per termination or per initiation. The radical chain length is a metric that refers solely to gas phase reactions (Monks, 2005). We have not, until the OASIS2009 campaign, had the high quality measurements available to enable a reliable estimation of the bromine radical chain length in the Arctic.

The length of the chain in a radical propagation cycle is limited by termination steps that destroy the chain carriers and result in relatively stable atmospheric species. Thus, the chain length can be defined as the rate of propagation divided by the rate of termination. Alternatively, the chain length can also be calculated using the rate of initiation. If the total bromine radical population is at steady-state, the rate of initiation is equal to the rate of termination; thus, for short-lived radical species, the two methods for calculating chain length should be approximately equal.

Method 1: $$\Phi = \frac{\Sigma(\text{Rates of propagation})}{\Sigma(\text{Rates of termination})} \quad (3)$$

Method 2: $$\Phi = \frac{\Sigma(\text{Rates of propagation})}{\Sigma(\text{Rates of initiation})} \quad (4)$$

We used our model to calculate the chain length for bromine radical propagation across the 7-days of the simulated period using both Method 1 and 2 as shown in Equations 5 and 6. Because bromine radicals are generated photolytically, the chain length is calculated for daytime only, defined here as approximately 7:00 to 20:00 Alaska Standard Time (AKST).

Method 1:
$$\Phi_{Br} = \frac{\begin{array}{l}(2k[BrO]^2 + J_{BrO}[BrO] + k[BrO][ClO] + \\ k[BrO][IO] + k[BrO][CH_3OO] + \\ k[BrO][OH] + k[BrO][O(^3P)] \\ + k[BrO][CH_3COOO] + k[BrO][NO])\end{array}}{\begin{array}{l}(k[Br][HO_2] + k[Br][C_2H_2] + k[Br][C_2H_4] \\ + k[Br][C_3H_6] + k[Br][HCHO] + k[Br][NO_2] \\ + k[Br][CH_3CHO] + k[Br][C_3H_6O] + k[Br][C_4H_8O] \\ + k[Br][CH_3OOH] + k[BrO][HO_2] + k[BrO][CH_3OO] \\ + k[BrO][C_3H_6O] + k[BrO][NO_2])\end{array}} \quad (5)$$

Method 2:
$$\Phi_{Br} = \frac{\begin{array}{l}(2k[BrO]^2 + J_{BrO}[BrO] + k[BrO][ClO] + \\ k[BrO][IO] + k[BrO][CH_3OO] + \\ k[BrO][OH] + k[BrO][O(^3P)] \\ + k[BrO][CH_3COOO] + k[BrO][NO])\end{array}}{\begin{array}{l}(k[Br][HO_2] + k[Br][C_2H_2] + k[Br][C_2H_4] \\ + k[Br][C_3H_6] + k[Br][HCHO] + k[Br][NO_2] \\ + k[Br][CH_3CHO] + k[Br][C_3H_6O] + k[Br][C_4H_8O] \\ + k[Br][CH_3OOH] + k[BrO][HO_2] + k[BrO][CH_3OO] \\ + k[BrO][C_3H_6O] + k[BrO][NO_2])\end{array}} \quad (6)$$

$$(2J_{Br2}[Br_2] + J_{BrCl}[BrCl] + J_{HOBr}[HOBr] + J_{BrONO2}[BrONO_2] + J_{IBr}[IBr] + J_{BrNO2}[BrNO_2] + J_{CHBR3}[CHBr_3] + k[HBr][OH] + k[CH_3Br][OH] + k[CHBr_3][OH])$$

Termination reactions for bromine include those reactions that are sinks for either Br and BrO, since Br and BrO rapidly interconvert. Here, photolysis of BrO and the BrO + NO reaction is included in the numerator because they are efficient at reforming Br and propagating the chain; however, these reactions do not result in a net loss of ozone. Photolysis of BrO produces atomic oxygen that reacts with O_2 to form O_3, and NO_2 can photolyze to similarly reform O_3. Therefore, it should be noted that if we omit these reactions and consider only those that result in a net O_3 loss, it would be expected that the chain length would be shorter. Indeed, model simulations were performed without these two terms and the determined chain lengths were on average 80% lower than those presented here. BrO reaction with CH_3OO is included in both the numerator and denominator in Equation 5 because this reaction has two channels, one that propagates the Br chain and one that terminates it.

In Figure 3, we present the hourly-averaged results of these calculations for the Base Model, which show that the two methods for calculating bromine chain length are in reasonably good agreement, although there are small differences between the two methods throughout the time-series. This agreement is a test of our basic understanding of the radical chemistry. The inset graph in Figure 3 shows a linear regression of the two methods for the chain length calculation. The coefficient of determination (r^2) of 0.93 confirms the good temporal agreement between the two methods. However, the slope of 0.68 indicates that Method 1 is generally higher than Method 2 throughout (with some periods of exception). This offset reveals that either Method 1 is slightly overestimating the chain length, or that Method 2 is underestimating it. The numerator is identical in Equations 5 and 6, therefore, the denominator must be driving this

457 discrepancy, with either the denominator term in Method 1 too low or the denominator term in
458 Method 2 too high (or some combination thereof). If it's the case that the Method 1 denominator
459 is too low, then it must be concluded that there are important BrO_x terminations that are missing
460 from the calculation. If, however, the denominator of Method 2 is too high, this would imply that
461 our measurements of these BrO_x precursors are too high, which, as discussed above, is a known
462 possibility at least for the Br_2 measurements. The photolysis of Br_2 is the dominant initiation
463 pathway (see Section 3.3), therefore, the Method 2 chain length calculation would be the most
464 sensitive to Br_2 measurement inaccuracies.

465 In Equation 6, we included photolysis of the most prevalent organobromine compound
466 bromoform for completeness, though it has been recognized for many years that the rate of Br
467 atom production from this pathway is small (e.g., ~ 100 molecules·cm^{-3}·s^{-1} for bromoform at
468 mid-day) compared to Br atom production from Br_2 photolysis (~1.3x10^7 molecules·cm^{-3}·s^{-1} at
469 mid-day assuming 5 pptv of Br_2). Photolysis of bromine nitrate ($BrONO_2$) and nitryl bromide
470 ($BrNO_2$) are also included, however, the prevalence of and production of these compounds in the
471 Arctic is highly uncertain, and no observations of these species in the Arctic have been published
472 to date with which to compare to our modeled mixing ratios. Inclusion of these terms at the
473 modeled $BrONO_2$ and $BrNO_2$ mixing ratios has a small effect on the calculated chain length that
474 cannot account for the discrepancy between the two methods.

475 The median bromine chain-length in the Base simulation, averaging the results from
476 Method 1 and Method 2, is ~1.2 across daylight hours (7:00 to 21:00 AKST) and ~2 for
477 afternoon hours, defined for this purpose as approximately 12:00 until 18:00 AKST, when $[O_3] \geq$
478 5 ppbv. In comparison, the bromine chain length is ~0.4 when $[O_3] < 5$ ppbv (Figure 3). In other
479 words, the chain cannot be maintained when $[O_3] < 5$ ppbv. Under these conditions, Br atoms

480 readily terminate, e.g. via reaction with CH_3CHO (see below). On 29 March there is an early
481 morning enhancement in the chain length. This morning spike appears to correlate with a similar
482 sharp increase in ozone. Br_2 accumulates during the nighttime hours, resulting in the highest Br_2
483 concentrations in the early morning hours (Figure 1B). When the sun rises, Br_2 photolyzes
484 rapidly, releasing a pulse of reactive bromine that converts to BrO in the presence of ozone. This,
485 in concert with the coincident increase in ozone, can explain the enhanced chain length during
486 the early morning hours.

487 Overall, midday bromine chain lengths remain near or below 2 during background O_3
488 days. This implies that, for these days, ozone depletion is strongly dependent upon initiation
489 processes, and most BrO radicals produced terminate the chain via reactions R5 and R10 (see
490 below) in less than two cycles. Reaction R12 (see below) will also efficiently terminate the chain,
491 however, the relative importance of R10 and R12 depend upon the relative abundances of BrO
492 and Br. For background O_3 days, such as 29 and 30 March, [BrO] > [Br], thus, R10 > R12. The
493 low chain lengths calculated here are surprising, given that it has been generally accepted that Br
494 is recycled efficiently in the gas-phase. That it appears this is not the case supports the
495 conclusions of Michalowski et al. (2000), Piot and von Glasow (2008), and Toyota et al. (2014)
496 that heterogeneous recycling through the "bromine explosion", which emits Br_2 and BrCl from
497 surface reactions, is of critical importance to sustain ODEs occurring at the surface.

498 A question to address regarding the relatively small chain length calculated for Br is to
499 what extent the chain length is dependent on NO_2. As discussed in Thompson et al. (2015) and
500 further investigated in Custard et al. (2015), NO_2 at Barrow can be greater and more variable
501 than at very remote sites due to its proximity to anthropogenic emissions sources. We find that
502 the chain length calculation is relatively insensitive to NO_2 concentrations and so it is robust for

503 the range of conditions encountered at Barrow. This is shown in detail in Custard et al. (2015).
504 As discussed by Custard and coworkers, while NO_2 can inhibit the bromine chain through
505 reactions R10 and R12 (i.e., decreasing the chain length), enhanced NO_2 will also reduce
506 available HO_2, thereby decreasing the HO_2 available to terminate the chain (i.e., increasing the
507 chain length). While the Method 2 calculation does not contain NO_2 in the denominator, the
508 absolute [BrO] is NO_x-dependent because of reaction R10 (Custard et al., 2015), and it is through
509 this effect that high NO_x mixing ratios act to decrease the rate of O_3 depletion. In the natural
510 environment, Br_2 production can potentially also be NO_x-dependent, e.g. via reaction R11,
511 followed by R7. While our model does not *simulate* the condensed phase processes, it is
512 implicitly sensitive to them, since the model is constrained to the product of those processes, Br_2.

513 $$BrO + NO_2 \rightarrow BrONO_2 \quad \text{(R10)}$$

514 $$BrONO_{2(aq)} + H_2O \rightarrow HOBr + HNO_3 \quad \text{(R11)}$$

515 $$Br + NO_2 \rightarrow BrNO_2 \quad \text{(R12)}$$

516 On the other hand, for the period of 26 through 30 March, NO_x was relatively low, and the
517 relatively good agreement between the two calculation methods further supports our conclusion.
518 To investigate how chemical interactions with chlorine and iodine affect the bromine
519 chain length, a series of simulations was performed by varying the combinations of halogens
520 present in the model. The bromine chain length was determined for scenarios with only Br, Br
521 and Cl (Base Model), Br and Iodine, and Base with Iodine. Simulations without chlorine were
522 performed simply by removing Cl_2, while simulations with iodine were performed by
523 incorporating the I_2 flux as described in Section 2.2. No other adjustments were made to the
524 model for these sensitivity runs.

525 Table 2 shows the results for both chain length calculation methods (i.e., Equations 5 and
526 6) for the different halogen combinations for the three days when ozone was present near
527 background values: 25, 29 and 30 March. For the Base scenario ("Br and Cl"), the average of the
528 median daily values for the bromine chain length is 1.43 and 1.05 for Method 1 and Method 2,
529 respectively. In comparison with the "Br Only" run, Cl chemistry does not induce a net increase
530 in the Br chain length, but rather causes a slight decrease. Cl chemistry can increase Br radical
531 propagation through the addition of the BrO + ClO cross-reaction and enhancement of the BrO +
532 CH_3OO radical propagation terms. However, Cl chemistry can also increase the concentration of
533 reactive bromine sinks, such as aldehydes (e.g., propanal and butanal, which were free to evolve
534 in our model; HCHO and CH_3CHO are fixed to observations) and HO_2 (see Thompson et al.,
535 2015). Iodine has the effect of increasing the Br chain length. When low levels of iodine are
536 added to the "Br Only" simulation, the chain increases from 1.52 to 1.59 in the Method 1
537 calculation, primarily due to the very fast cross-reaction between IO and BrO. The addition of
538 Cl to the "Br and I" simulation imparts a slight decrease to the Br chain length. This may be
539 explained by the competition between BrO and ClO for reaction with NO and/or IO, as well as
540 the additional Br sinks in the presence of Cl chemistry. Regardless, overall there is more Br
541 available for reaction with O_3 when Cl is present due to the interhalogen reactions, thereby
542 increasing the rate of ozone depletion (see Thompson et al., 2015 for further discussion on ozone
543 depletion rates).

544 There are several conclusions that can be drawn from Figure 3 and Table 2: 1) there is a
545 distinct difference in bromine chain length between O_3-depleted and non-depleted days with a
546 significantly larger chain length when ozone is present, and 2) for all simulations, the average
547 bromine chain is much shorter than often expected (given that gas-phase recycling has, to date,

548 been assumed to be highly efficient). The chain length is greatest when ozone is present because
549 many of the species that propagate the Br chain (e.g., BrO, ClO, IO, and to a lesser extent OH
550 and CH_3OO) require O_3 for production. Although the relationship between bromine chain length
551 and BrO is not straightforward due to the multitude of interactions between BrO and other
552 species that either propagate or terminate the chain, the chain length does exhibit a rough
553 dependence on [BrO], as shown in Figure 4, that can be loosely described with a linear fit. If it
554 were the case that the gas-phase Br chain length was relatively long (such that the numerator far
555 outweighs the denominator), and dominated by the BrO self-reaction, the numerator in Equations
556 5 and 6 would reduce to $2k[BrO]^2$, and the regression in Figure 4 would display a quadratic fit;
557 however, that is not observed here.

558 For purposes of comparison, the chain lengths for Cl and I were also calculated in a
559 manner analogous to that of Equation 5. These results are shown as hourly averages in Figure 5
560 for the Base with Iodine scenario. It is apparent from this figure that reactive chlorine exhibits
561 an exceptionally short chain length, whereas reactive iodine has a relatively long chain length.
562 The average Cl chain length across the three days of background ozone (25, 29, and 30 March) is
563 0.15, or 0.23 considering only afternoon hours (12:00 – 18:00 AKST). This result indicates that
564 nearly all Cl atoms that are produced terminate, likely through the very efficient reaction with a
565 multitude of VOCs, as shown in Thompson et al. (2015). This behavior also helps explain why
566 Cl has only a small effect on the bromine chain length. In contrast, I and IO have few known
567 sinks, which results in a reactive iodine chain length of 5.7 on average over 25, 29, and 30 March,
568 and 7.3 over only mid-day hours, with maxima over 12. The high efficiency of the gas-phase
569 regeneration of I in part explains why iodine is more efficient on a per atom basis at depleting
570 ozone than either Br or Cl (Thompson et al., 2015).

571

572 **3.3 Reactive bromine initiation, propagation, and termination pathways**

573 The individual reactions that initiate, propagate, and terminate the reactive bromine chain
574 were examined to determine the most important reaction pathways contributing to the chain
575 reactions. The rates of Br atom production from the most important initiation pathways are
576 shown as hourly averages in Figure 6, with the y-axes expressed as the cumulative rate of
577 reaction, including all five precursors. These are reactions that produce Br atoms from stable
578 reservoir species, which is an important distinction from the propagation reactions that produce
579 Br atoms through radical reactions. Br_2 photolysis is calculated as 2 x $J_{Br2}[Br_2]$. Here, we do not
580 separate Br_2 produced in the gas-phase versus that directly emitted from a surface (this will be
581 discussed further in Section 3.5). The contribution of Br_2 photolysis in producing Br atoms vastly
582 dominates the cumulative production rate (Figure 6A). Therefore, in Figure 6B we show the
583 initiation terms without Br_2 photolysis so that these other production pathways can be visualized.

584 Effectively, Br_2 photolysis alone controls the production of bromine atoms, while the
585 remaining initiation pathways combined add only a minor contribution. Among the minor
586 pathways, HOBr photolysis is the most significant during non-ODE days, with the exception of
587 the high NO_x period of March 25, where $BrNO_2$ has the largest impact. In a highly polluted
588 environment, halogen cycling through NO_x reservoirs would become significantly more
589 important, as has been observed with $ClNO_2$ in mid-latitude regions (Thornton et al., 2010;
590 Mielke et al., 2011; Young et al., 2012). The small contribution of HOBr photolysis to bromine
591 atom production is an important point, because the gas-phase BrO + HOBr → BrO + HO_2 ozone
592 depletion cycle (that proceeds via HOBr photolysis rather than surface deposition) has been
593 considered to be significant previously (see, e.g., Hausmann and Platt, 1994), though Zeng et al.

(2006) note that HOBr photolysis has only a small effect on BrO_x cycling. Using the version of our model that is unconstrained to HOBr, but incorporates a larger surface deposition in order to reproduce observations (Figure 2C), we were able to determine that photolysis accounts for 19% of the HOBr sink integrated over the 7-day simulation period. Surface deposition accounts for 80%, and other known gas-phase reactions (HOBr + Br, HOBr + Cl, HOBr + OH, HOBr + O) are only minor sink terms at a combined 1%.

The cumulative rates of reaction of the most important propagation pathways, with and without iodine, are shown in Figure 7 A and B. The rate of the BrO + BrO reaction is calculated as $2k[BrO]^2$, since this reaction results in the production of two Br atoms. The reaction pathways that dominate the bromine propagation, i.e., BrO photolysis and reaction with NO, are those that do not result in a net ozone loss. This has been previously recognized and applied to Br steady-state calculations in several works (e.g., Platt and Janssen, 1995; Zeng et al., 2006; Holmes et al., 2010), and demonstrates that much of the time BrO regenerates Br without a net loss of ozone for the simulated conditions in Barrow. Indeed, in our previous paper, we calculated that ~70% of gas-phase BrO reforms ozone via photolysis or reaction with NO over this period (Thompson et al., 2015). The inset pie charts, which show the average fractional importance of the various propagation reactions for 29 and 30 March, reveal that these two pathways account for 88 – 91% of the total. Interestingly, the BrO self-reaction is small in comparison, with an average contribution of 5 – 6%, and a maximum of 46%. However, if we consider only those reactions that *do* lead to a net ozone loss, then the BrO self-reaction accounts for an average of 71% and a maximum of 98% of the propagation. The rate of the BrO + ClO reaction rate is much smaller than that for BrO + BrO, though not insignificant. While on average this reaction pathway accounts for only 2%, it does reach 16% when Cl_2 is high on 29 March. In considering only

617 those reactions that result in a net ozone loss, the BrO + ClO pathway accounts for 21% on
618 average, and up to a maximum of 57%. In Panel B, the Base with Iodine scenario is shown. At
619 these levels, the BrO + IO reaction accounts for 4% of the propagation, which is at times
620 comparable to BrO + BrO and greater than BrO + ClO, even at the low IO mixing ratios in this
621 simulation (~1 pptv).

622 The short gas-phase chain length calculated for bromine propagation indicates that there
623 are large reactive bromine (BrO_x) sinks terminating the chain reaction. Figure 8 presents the
624 rates of the most important BrO_x termination reactions, with the y-axis expressed as the
625 cumulative rate of reaction. Here it can be seen that reaction of BrO with NO_2 is the dominant
626 sink for BrO_x on non-ODE days for the conditions encountered at Barrow, while Br reaction with
627 CH_3CHO is most important when O_3 is depleted. That HO_2 is a significant sink, and would be
628 more so in less anthropogenically-impacted Polar Regions, points toward the importance of
629 heterogeneous recycling through the bromine explosion mechanism. During ozone depletion,
630 such as the major event from days 26 – 28 March ($[O_3] < 5$ppbv) when BrO is mostly absent,
631 CH_3CHO becomes the primary sink term for Br, and HCHO is relatively more important. The
632 strength of the CH_3CHO sink is much greater than is HCHO, as noted previously by Shepson et
633 al. (1996) and Bottenheim et al. (1990). Of note are the relatively similar magnitudes for the
634 total rate of reaction of the initiation, propagation, and termination reactions shown in Figures 6,
635 7, and 8, respectively, which of course must be the case for a chain length near 1. This accounts
636 for the short bromine chain length determined here and also indicates that to sustain elevated
637 bromine radical concentrations necessary to deplete O_3 requires a relatively large Br_2 source,
638 likely in the form of a significant flux of Br_2 from the snow surface, or from in-situ production
639 from aerosols.

640

641 **3.4 Ozone loss rate**

642 Since the chain length calculations suggest a larger than expected contribution of
643 heterogeneous bromine recycling to Br atom production, to examine this further, we calculated
644 the rate of net ozone loss by Br and Cl in the Base Model using Equation 7 and compared this
645 rate to that using the estimation method presented in previous works as shown in Equation 2
646 (Platt and Janssen, 1995; Le Bras and Platt, 1995). Additionally, the total simulated chemical
647 ozone loss in the Base Model was calculated from Equation 8, which includes O_3 destruction by
648 OH, HO_2, and photolysis (determined here as $k[O(^1D)][H_2O]$).

649 $$O_3 \text{ Loss by Br and Cl} = (k[Br][O_3] - J[BrO] - k[BrO][NO]) \quad (7)$$
650 $$+ (k[Cl][O_3] - J[ClO] - k[ClO][NO])$$

651 $$\text{Total Chemical } O_3 \text{ loss rate} = k[Br][O_3] + k[Cl][O_3] + k[O(^1D)][H_2O] \quad (8)$$
652 $$+ k[OH][O_3] + k[HO_2][O_3] - k[BrO][NO]$$
653 $$- J[BrO] - k[ClO][NO] - J[ClO]$$

654 The method in Equation 2 assumes that the rate of ozone loss is equivalent to the rate at which
655 Br is regenerated through BrO reaction with itself and ClO (thus assuming efficient gas-phase
656 propagation and a long chain length), whereas Equation 7 accounts for all net ozone destruction
657 by Br and Cl, by correcting for those reactions that release a triplet oxygen atom and reform O_3.
658 In other words, this method accounts for the fact that some BrO radicals react to terminate the
659 chain (and at steady state, an equivalent BrO_x production rate is necessary). Figure 9A compares
660 these two estimations for O_3 loss rate in green (Equation 2) and pink (Equation 7). This
661 comparison clearly shows that there is a large difference between the methods, with the
662 estimation from Equation 2 significantly smaller overall. Additionally, the total chemical O_3 loss
663 (calculated by Equation 8) is shown in the dashed black trace. The O_3 loss rate estimation
664 presented in Equation 7 accounts for nearly all of the chemical O_3 loss (i.e., most chemical O_3

loss is a result of halogen chemistry), such that the dashed black line lies nearly perfectly on top of the pink shaded regions.

In Figure 9B, we show a regression of the two estimation methods (Equation 2 in green and Equation 7 in pink) versus the total chemical O_3 loss rate (Equation 8). Here it can be seen from the pink data that halogen chemistry accounts for 99% of the total chemical O_3 loss under the conditions simulated here. Importantly, the O_3 loss rate estimation presented in Equation 2 accounts for only 44% of the total chemical O_3 loss rate.

In the 1994 work by Hausmann and Platt, the authors also considered the BrO + HO → Br + HO_2 gas-phase ozone depletion cycle as a proxy for estimating the O_3 loss rate, using the equation shown below (Equation 17 of Hausmann and Platt, 1994).

$$-\frac{d[O_3]}{dt} = (k_5 \cdot [BrO] \cdot [HO_2]) \quad (9)$$

The authors only considered the gas-phase cycle of HOBr here with the photolysis of HOBr regenerating Br. At the time of this publication, the heterogeneous cycling of HOBr had only recently been proposed and had not been fully validated. Hausmann and Platt showed that Equation 9 resulted in a significantly lower estimation for O_3 depletion than did Equation 1, which considered only the BrO-BrO cycle. In Figure 9B, we show also the O_3 loss rate estimated using Equation 9 in blue. Our results corroborate that of Hausmann and Platt (1994), and demonstrate that Equation 9 can account for only 18% of the O_3 loss. To examine this one step further, we present an additional regression in Figure 8B (orange trace) that combines Equations 2 and 9, thereby considering the three predominant gas-phase O_3 depletion cycles of BrO-BrO, BrO-ClO, and BrO-HO_2. This still can only account for 60% of the O_3 loss.

Our analysis quantitatively expresses the conclusion that the gas-phase recycling of bromine is not as efficient as previously considered and that it is often the case, for Barrow, that

688 BrO_x terminations must often, through reactions R5 or R10, be followed by heterogeneous
689 production of Br_2 through condensed-phase reactions of HOBr and/or $BrONO_2$. In other words,
690 the reproduction of Br_2 via reactive deposition/uptake of HOBr and/or $BrONO_2$ onto surfaces,
691 followed by their gas-phase production via BrO + HO_2 and BrO + NO_2, respectively, plays a
692 significant role in the catalytic ozone loss involving Br atoms in the Arctic boundary layer. An
693 important conclusion from this analysis is that the chemical O_3 loss rate is largely underestimated
694 when calculated from only BrO observations using the previously accepted $2(k[BrO]^2$ +
695 [BrO][ClO]) method, and one should be cautious about drawing conclusions about O_3 depletion
696 rates and timescales based solely on BrO observations. This may have significant impacts on the
697 process of examining ODEs and addressing the extent to which they represent local scale
698 chemistry versus transport effects. While this situation is significantly impacted by local NO_x
699 sources at Barrow, NO_x is expected to increase with development around the Arctic.
700
701 **3.5 Bromine atom production**
702 If it is the case that heterogeneous recycling is of such importance, it may be that
703 Reaction R5 (BrO + HO_2) competes favorably with Reaction R3 (BrO + BrO). Panel A of
704 Figure 10 shows the rates of reactions R5 and R3. This plot demonstrates that for our modeling
705 results the rate of reaction of BrO with HO_2 is often of a comparable or greater magnitude than
706 the BrO self-reaction, and remains significant throughout the simulated period. Previous
707 modeling work by Sander et al. (1997) also compared the rates of these two critical reactions
708 (Figure 2 of that work). In contrast to our results, their model predicted that the rate of the BrO +
709 BrO reaction was up to a factor of 8 greater than that of BrO + HO_2. The reason for this
710 difference may perhaps be the much lower mixing ratios of HO_2 in the model by Sander and

711 coworkers. Their model predicted HO_2 daily maxima of 0.2 to 0.6 pptv for most days, increasing
712 to 1.8 pptv on the final three days of their simulation. In contrast, HO_2 observations at Barrow
713 were frequently greater than 5 pptv and up to 10 pptv. As demonstrated in Thompson et al.
714 (2015), HCHO was a dominant factor in controlling the HO_2 mixing ratios in Barrow. The low
715 levels of HO_2 in Sander et al. (1997) likely also contribute to their low predicted HOBr mixing
716 ratios, which do not exceed 1 pptv in their model. This also is much lower than observations at
717 Barrow, where HOBr reaching 10 pptv to 20 pptv was measured during our simulated period.
718 Because the BrO + HO_2 reaction is of primary importance for the bromine explosion mechanism,
719 our result supports the hypothesis that heterogeneous recycling may be equally or even more
720 important than gas-phase recycling of reactive bromine.

721 Given that the chain length is small, it must be that initiation is an important source of Br
722 atoms in order to sustain BrO and lead to O_3 depletion. To further examine the question of
723 surface emissions/release versus gas-phase recycling, we determined the rate of production of Br
724 atoms via photolysis of Br_2 and BrCl (Equation 10) compared to the rate of production of Br
725 atoms through gas-phase recycling calculated by Equation 11. Because our model is constrained
726 by Br_2 observations and we do not produce Br_2 from surfaces via heterogeneous reactions, the
727 photolysis of Br_2 includes Br_2 that is both emitted from surfaces and that is formed via gas-phase
728 reactions. To correct for the Br_2 that is formed in the gas-phase reactions so that Equation 10
729 represents our best approximation for surface-emitted Br_2, we created a proxy in the model, Br_2*,
730 that represents the Br_2 produced from gas phase reactions. These reactions include Br + $BrNO_2$,
731 Br + $BrONO_2$, and the BrO + BrO branch that produces Br_2. Equation 10 is thus corrected for the
732 gas-phase generated Br_2 by subtracting the photolysis of Br_2*. A comparison of Br_2 and Br_2*
733 reveals that these three gas-phase production pathways account for an average of 35% of

observed Br_2, suggesting that the snowpack and/or aerosols emits the remaining 65%. Again, we cannot distinguish between snow or aerosol production using this method.

$$\textit{Br Production from Surface-derived } Br_2, BrCl = 2 \times J_{Br2}[Br_2] + J_{BrCl}[BrCl] - 2 \times J_{Br2}[Br_2^*] \quad (10)$$

$$\begin{aligned} \textit{Br Production via Gas-phase Recycling} = {} & 2k[BrO][BrO] + k[BrO][ClO] \\ & + k[BrO][NO] + k[BrO][OH] + k[BrO][O(^3P)] \\ & + k[BrO][CH_3OO] + k[BrO][CH_3COOO] \\ & + J_{HOBr}[HOBr] + J_{BrO}[BrO] + J_{BrONO2}[BrONO_2] \\ & + J_{BrNO2}[BrNO_2] \end{aligned} \quad (11)$$

Panel B of Figure 10 compares the results of Equations 10 and 11, showing the total rate of Br atom production separated into Br production from the derived "surface-emitted" Br_2 and BrCl (purple) and from gas-phase Br recycling (orange); Panel C plots the fraction of total Br atom production that is due to production from Br_2 and BrCl surface emissions/release. The majority of the time during this 7-day period Br atom production from Br_2 and BrCl emissions/release (Equation 10) accounts for 30% or greater of the total, and at times reaches up to 90%. This explains both how ozone depletion can be rapid despite the short calculated bromine radical chain length, as well as the difference found between the two methods of estimating O_3 loss rate in Figure 9. It is concluded from this analysis, then, that the condensed phase recycling of bromine can be of equal or greater importance to the evolution of ODEs than gas-phase Br regeneration through radical recycling reactions.

4 Conclusions

The analysis presented here suggests that the gas-phase recycling of bromine species may be less important than commonly believed, and we conclude that heterogeneous recycling is critical for the evolution of ODEs/AMDEs, consistent with results by Michalowski et al. (2000),

762 Piot and von Glasow (2008), and Toyota et al. (2011, 2014). Expressed in another way, the
763 reproduction of Br_2 via reactive deposition/uptake of HOBr and/or $BrONO_2$ onto surfaces,
764 followed by their gas-phase production via BrO + HO_2 and BrO + NO_2, respectively, is critical
765 for sustaining the Br atom chemistry leading to O_3 depletion in the Arctic boundary layer.

766 To support this conclusion, we have used the gas-phase bromine chain length, which has
767 not previously been applied to Arctic halogen chemistry, as an objective metric. The gas-phase
768 bromine chain length is much shorter than expected, suggesting that much of the Br present in
769 the gas-phase is Br from surface emissions/release. Again note that our calculation of chain
770 length includes photolysis of BrO and BrO + NO, which do not result in net O_3 loss. Had we
771 omitted these two reactions, which we have found are in fact dominating the radical propagation,
772 the chain length would be, on average, 80% shorter. Because of the small chain length calculated
773 for Br, one must be cautious about drawing conclusions about O_3 depletion from BrO
774 measurements alone. We recommend concurrent measurements of a broad suite of inorganic
775 bromine species for accurate study of these ozone depletion events. The very low mixing ratios
776 of HOBr predicted by Sander et al. (1997) and the high mixing ratios originally predicted by our
777 model point to the need for measurements of these species to validate the accuracy of Arctic
778 models.

779 We find that between 30 – 90% of Br atoms are produced from surface emissions/release
780 of Br_2 and BrCl, though we cannot distinguish snow sources from aerosol sources using our
781 model. However, it is important to note that we do not know how much of the condensed phase
782 Br_2 production derives from reaction R7, or from some other condensed phase process, e.g.
783 oxidation of Br^- by OH radicals (Abbatt et al., 2010). The in situ snow chamber experiments by
784 Pratt et al. (2013) demonstrate a strong Br_2 source from the snowpack; similar field observations

785 proving significant Br_2 release from Arctic aerosol are currently lacking. If the snow surface is
786 the primary sources of these emissions, then a strong vertical gradient would be expected in the
787 near surface boundary layer, and our estimations for the Br chain length would be only valid for
788 the height of our measurements (~ 1 m above the snow). Strong deposition to the snow would
789 also induce a vertical gradient in these species. If, however, aerosols are an important source of
790 Br_2 (or other halogen precursors), then Br_2 production should occur throughout the entire height
791 of the boundary with no significant vertical gradient, in a similar fashion as has been observed
792 for $ClNO_2$, which is a known product of aerosol chemistry (Young et al., 2012). It is clear that
793 vertically-resolved measurements of these halogen precursors are imperative for our
794 understanding of halogen production in the Arctic.

795 The production of Br_2 is quite complex and is dependent on many factors, including the
796 relative concentrations of bromide and chloride (among others), the availability of atmospheric
797 oxidants, such as ozone (e.g., Oum et al., 1998; Pratt et al., 2013), the pH of the snow surfaces or
798 aerosol (Toyota et al., 2011, 2014), the presence of snow phase oxidants such as H_2O_2 (Pratt et
799 al., 2013), and the replenishment of the snowpack halides from deposited sea salts. The last of
800 these is governed by meteorology, the proximity of open water or saline sea ice surfaces, and
801 wind/storm events, making the accurate modeling of these processes very complex (Domine et
802 al., 2013). Likewise, to date, it has not been possible to determine the halide concentrations or
803 pH of the snow grain surfaces, and these values are likely highly variable and dependent on snow
804 and aerosol aging and deposition of atmospheric constituents. Due to the apparent importance of
805 surface chemistry for both the initiation and evolution of Arctic ozone depletion events, it is clear
806 that more laboratory and field studies are required to decipher these complex chemical and
807 physical processes. In particular, we strongly recommend studies relating to direct

808 measurements of surface fluxes of molecular halogens, as a function of conditions of temperature,
809 snowpack composition, and pH, as well as deposition velocities for the hypohalous acids (HOBr,
810 HOCl) to the snow. Our model overestimation of HOBr, that necessitated constraint to
811 observations, suggests a sometimes much stronger, but also variable, deposition of HOBr that is
812 currently unknown. Further, there is currently little understanding of the mechanism for Cl_2
813 production in the Arctic, and no successful measurements of IO in the High Arctic. Recent
814 observations of I_2 within the Barrow snowpack (Raso et al., 2016) suggest reactive iodine
815 chemistry is present in this region, and this would have an impact on Br recycling and ozone
816 depletion rate. Investigations into these areas would greatly increase our understanding of
817 halogen chemistry and ozone depletion in the Arctic.
818
819 **Acknowledgements** This work was funded by the National Science Foundation grant ARC-
820 0732556. Partial support for CT during preparation of this manuscript was provided by the NSF
821 Atmospheric and Geospace Sciences Postdoctoral Research Fellowship program. The authors
822 wish to thank the organizers of the OASIS 2009 field campaign, the Barrow Arctic Science
823 Consortium for logistics support, and all of the researchers who contributed to the campaign.
824 This paper is submitted in memory of our colleague and friend, Roland von Glasow.
825
826
827
828 **References**

829 Abbatt, J., Oldridge, N., Symington, A., Chukalovskiy, V., McWhinney, R. D., Sjostedt, S. and
830 Cox, R. A.: Release of Gas-Phase Halogens by Photolytic Generation of OH in Frozen
831 Halide−Nitrate Solutions: An Active Halogen Formation Mechanism?, J. Phys. Chem. A,
832 114(23), 6527–6533, doi:10.1021/jp102072t, 2010.
833

834 Abbatt, J. P. D., Thomas, J. L., Abrahamsson, K., Boxe, C., Granfors, A., Jones, A. E., King, M.
835 D., Saiz-Lopez, A., Shepson, P. B., Sodeau, J., Toohey, D. W., Toubin, C., von Glasow, R.,
836 Wren, S. N., and Yang, X.: Halogen activation via interactions with environmental ice and snow
837 in the polar lower troposphere and other regions, Atmos. Chem. Phys., 12, 6237-6271, 2012.
838
839 Adams, J., Holmes, N., and Crowley, J.: Uptake and reaction of HOBr on frozen and dry
840 NaCl/NaBr surfaces between 253 and 233K, Atmos. Chem. Phys., 2, 79 – 91, doi: 10.5194/acp-
841 2-79-2002, 2002.
842
843 Ariya, P., Jobson, B., Sander, R., Niki, H., Harris, G., Hopper, J., and Anlauf, K.: Measurements
844 of C2-C7 hydrocarbons during the Polar Sunrise Experiment 1994: Further evidence for halogen
845 chemistry in the troposphere, J. Geophys. Res., 103, 13169-13180, 1998.
846
847 Atkinson, R., Baulch, D. L., Cox, R. A., Crowley, J. N., Hampson, R. F., Hynes, R. G., Jenkin,
848 M. E., Rossi, M. J. and Troe, J.: Evaluated kinetic and photochemical data for atmospheric
849 chemistry: Volume II gas phase reactions of organic species, Atmos. Chem. Phys., 6, 3625-4055,
850 2006.
851
852 Atkinson, R., Baulch, D. L., Cox, R. A., Crowley, J. N., Hampson, R. F., Hynes, R. G., Jenkin,
853 M. E., Rossi, M. J. and Troe, J.: Evaluated kinetic and photochemical data for atmospheric
854 chemistry: Volume III gas phase reactions of inorganic halogens, Atmos. Chem. Phys., 7, 981-
855 119, 2007.
856
857 Barrie, L., Bottenheim, J., Schnell, R., Crutzen, P., and Rasmussen, R.: Ozone destruction and
858 photochemical reactions at polar sunrise in the lower Arctic atmosphere, Nature, 334, 138 - 141,
859 doi: 10.1038/334138a0, 1988.
860
861 Bottenheim, J.W., Barrie, L. A., Atlas, E., Heidt, L. E., Niki, H., Rasmussen, R. A., and Shepson,
862 P.B.: Depletion of lower tropospheric ozone during Arctic spring: The Polar Sunrise Experiment
863 1998, J. Geophys. Res., 95, 18555-18568, 1990.
864
865 Calvert, J. G., and Lindberg, S. E.: Potential influence of iodine-containing compounds on the
866 chemistry of the troposphere in the polar spring. I. Ozone depletion, Atmos. Environ., 38, 5087-
867 5104, doi: 10.1016/j.atmosenv.2004.05.049, 2004.
868
869 Cao, L., Sihler, H., Platt, U., and Gutheil, E.: Numerical analysis of the chemical kinetic
870 mechanisms of ozone depletion and halogen release in the polar troposphere, Atmos. Chem.
871 Phys., 14, 3771-3787, 2014.
872
873 Carpenter, L. J., S. M. MacDonald, M. D. Shaw, R. Kumar, R.W. Saunders, R. Parthipan,
874 J.Wilson and J. M. C. Plane, Atmospheric iodine levels influenced by sea surface emissions of
875 inorganic iodine, Nature Geosci*., 6,* 108-111, doi: 10.1038/ngeo1687, 2013.

876 Cavender, A., Biesenthal, T., Bottenheim, J., and Shepson, P.: Volatile organic compound ratios
877 as probes of halogen atom chemistry in the Arctic, Atmos. Chem. Phys., 8, 1737-1750, 2008.
878

879 Custard, K. D., Thompson, C. R., Pratt, K. A., Shepson, P. B., Liao, J., Huey, L. G., Orlando, J.
880 J., Weinheimer, A. J., Apel, E., Hall, S. R., Flocke, F., Mauldin, L., Hornbrook, R. S., Pöhler, D.,
881 General, S., Zielcke, J., Simpson, W. R., Platt, U., Fried, A., Weibring, P., Sive, B. C., Ullmann,
882 K., Cantrell, C., Knapp, D. J., and Montzka, D. D.: The NOx dependence of bromine chemistry
883 in the Arctic atmospheric boundary layer, Atmos. Chem. Phys., 15, 10799-10809, 2015.
884
885 Domine, F., J. Bock, D. Voisin, and D. J. Donaldson, Can We Model Snow Photochemistry?
886 Problems with the Current Approaches, J. Phys. Chem., A, 117, 4733−4749, doi:
887 10.1021/jp3123314, 2013.
888
889 Edwards, G. D., Cantrell, C. A., Stephens, S., Hill, B., Goyea, O., Shetter, R. E., Mauldin III, R.
890 L., Kosciuch, E., Tanner, D. J., and Eisele, F. L.: Chemical ionization mass spectrometer
891 instrument for the measurement of tropospheric HO_2 and RO_2, Anal. Chem., 75, 5317-5327, doi:
892 10.1021/ac034402b, 2003.
893
894 Ehhalt, D. H.: Photooxidation of trace gases in the troposphere Plenary Lecture, Phys. Chem.
895 Chem. Phys., 1, 5401-5408, 1999.
896
897 Fan, S-M. and D. J. Jacob, Surface ozone depletion in Arctic spring sustained by bromine
898 reactions on aerosols, Nature, 358, 522-524, 1992.
899
900 Foster, K. L., Plastridge, R. A., Bottenheim, J. W., Shepson, P. B., Finlayson-Pitts, B. J., and
901 Spicer, C. W.: The role of Br_2 and BrCl in surface ozone destruction at polar sunrise, Science,
902 291, 471-474, 2001.
903
904 Frieß, U., Deutschmann, T., Gilfedder, B., Weller, R., and Platt, U.: Iodine monoxide in the
905 Antarctic snowpack, Atmos. Chem. Phys, 10, 2439-2456, 2010.
906
907 Gladich, I., J. S. Francisco, R. J. Buszek, M. Vazdar, M. A. Caignano, and P. B. Shepson, *Ab*
908 *Initio* Study of the Reaction of Ozone with Bromide Ion, J. Phys. Chem. A, 119, 4482−4488,
909 2015.
910
911 Gong, S., Walmsley, J., Barrie, L., and Hopper, J.: Mechanisms for surface ozone depletion and
912 recovery during polar sunrise, Atmos. Environ., 31, 969-981, 1997.
913
914 Guimbaud, C., Grannas, A. M., Shepson, P. B., Fuentes, J. D., Boudries, H., Bottenheim, J. W.,
915 Dominé, F., Houdier, S., Perrier, S., and Biesenthal, T. B.: Snowpack processing of acetaldehyde
916 and acetone in the Arctic atmospheric boundary layer, Atmos. Environ., 36, 2743-2752, 2002.
917
918 Hausmann, M., and Platt, U.: Spectroscopic measurement of bromine oxide and ozone in the
919 high Arctic during Polar Sunrise Experiment 1992, J. Geophys. Res., 99, 25399, 1994.
920
921 Helmig, D., Ganzeveld, L., Butler, T., and Oltmans, S.: The role of ozone atmosphere-snow gas
922 exchange on polar, boundary-layer tropospheric ozone? a review and sensitivity analysis, Atmos.
923 Chem. Phys., 7, 15-30, 2007.
924

925 Helmig, D., Boylan, P., Johnson, B., Oltmans, S., Fairall, C., Staebler, R., Weinheimer, A.,
926 Orlando, J., Knapp, D. J., Montzka, D. D., Flocke, F., Frieß, U., Sihler, H., and Shepson, P. B.:
927 Ozone dynamics and snow-atmosphere exchanges during ozone depletion events at Barrow,
928 Alaska, J. Geophys. Res., 117, D20303, doi:10.1029/2012JD017531, 2012.
929
930 Hirokawa, J., Onaka, K., Kajii, Y., and Akimoto, H.: Heterogeneous processes involving sodium
931 halide particles and ozone: molecular bromine release in the marine boundary layer in the
932 absence of nitrogen oxides, Geophys. Res. Lett., 25, 2449-2452, 1998.
933
934 Holmes, C. D., Jacob, D. J., Corbitt, E. S., Mao, J., Yang, X., Talbot, R., and Slemr, F.: Global
935 atmospheric model for mercury including oxidation by bromine atoms, Atmos. Chem. Phys., 10,
936 12037-12057, 2010.
937
938 Hönninger, G.: Halogen Oxide Studies in the Boundary Layer by Multi Axis Differential Optical
939 Absorption Spectroscopy and Active Longpath-DOAS, Ph.D., University of Heidelberg, 2002.
940
941 Huff, A. K., and Abbatt, J. P. D.: Kinetics and product yields in the heterogeneous reactions of
942 HOBr with ice surfaces containing NaBr and NaCl, J. Phys. Chem. A, 106, 5279-5287, 2002.
943
944 Jacob, D. J.: Heterogeneous chemistry and tropospheric ozone, Atmos. Environ., 34, 2131-2159,
945 2000.
946
947 Jobson, B., Niki, H., Yokouchi, Y., Bottenheim, J., Hopper, F., and Leaitch, R.: Measurements
948 of C2-C6 hydrocarbons during the Polar Sunrise 1992 Experiment: Evidence for Cl atom and Br
949 atom chemistry, J. Geophys. Res., 99, 25355-25368, 1994.
950
951 Kukui, A., Kirchner, U., Benter, T., and Schindler, R. N.: A gas kinetic investigation of HOBr
952 reactions with Cl(^{2}P), O(^{3}P) and OH(^{2}II). The reaction of BrCl with OH(^{2}II), Berichte Der
953 Bunsen-Gesellschaft-Physical Chemistry Chemical Physics, 100, 455-461, 1996.
954
955 Kuo, K. K.: Principles of combustion, John Wiley & Sons, New York, 1986.
956
957 Lary, D.: Gas phase atmospheric bromine photochemistry, J. Geophys. Res., 101, 1505-1516,
958 1996.
959
960 Le Bras, G., and Platt, U.: A possible mechanism for combined chlorine and bromine catalyzed
961 destruction of tropospheric ozone in the Arctic, Geophys. Res. Lett., 22, 599-602, 1995.
962
963 Lehrer, E., Hönninger, G., and Platt, U.: A one dimensional model study of the mechanism of
964 halogen liberation and vertical transport in the polar troposphere, Atmos. Chem. Phys., 4, 2427-
965 2440, 2004.
966
967 Liao, J., Huey, L., Scheuer, E., Dibb, J., Stickel, R., Tanner, D., Neuman, J., Nowak, J., Choi, S.,
968 and Wang, Y.: Characterization of soluble bromide measurements and a case study of BrO
969 observations during ARCTAS, Atmos. Chem. Phys, 12, 1327-1338, 2012a.
970

971 Liao, J., Huey, L., Tanner, D., Flocke, F., Orlando, J., Neuman, J., Nowak, J., Weinheimer, A.,
972 Hall, S., Smith, J., Fried, A., Staebler, R., Wang, Y., Koo, J.-H., Cantrell, C., Weibring, P.,
973 Walega, J., Knapp, D., Shepson, P., and Stephens, C.: Observations of inorganic bromine (HOBr,
974 BrO, and Br_2) speciation at Barrow, Alaska, in spring 2009, J. Geophys. Res., 117, D00R16,
975 2012b.
976
977 Liao, J., L. G. Huey, Z. Liu, D. J. Tanner, C. A. Cantrell, J. J. Orlando, F. M. Flocke, P. B.
978 Shepson, A. J. Weinheimer, S. R. Hall, H. J. Beine, Y. Wang, E. D. Ingall, C. R. Stephens, R. S.
979 Hornbrook, E. Apel, A. Fried, L. Mauldin, J. N. Smith, R. M. Staebler, J.A. Neuman, J.B.
980 Nowak, High levels of molecular chlorine in the Arctic atmosphere, Nature Geosci., 7, 91 – 94,
981 doi:10.1038/ngeo2046, 2014.

982 Mahajan, A., Shaw, M., Oetjen, H., Hornsby, K., Carpenter, L., Kaleschke, L., Tian-Kunze, X.,
983 Lee, J., Moller, S., and Edwards, P.: Evidence of reactive iodine chemistry in the Arctic
984 boundary layer, J. Geophys. Res., 115, D20303, doi: 10.1029/2009JD013665, 2010.
985
986 Mallard, W. G., Westley, F., Herron, J. T., Hampson, R. F., and Frizzel, D. H.: NIST Chemical
987 Kinetics Database: Version 5.0 National Institute of Standards and Technology, Gaithersburg,
988 MD. , 1993.

989
990 Martinez, M., Arnold, T., and Perner, D.: The role of bromine and chlorine chemistry for arctic
991 ozone depletion events in Ny-Ålesund and comparison with model calculations, Annales
992 Geophysicae, 17, 941-956, 1999.
993
994 McFiggans, G., Plane, J. M. C., Allan, B. J., Carpenter, L. J., Coe, H., and O'Dowd, C.: A
995 modeling study of iodine chemistry in the marine boundary layer, J. Geophys. Res., 105, 14371-
996 14385, 2000.
997
998 McFiggans, G., Cox, R. A., Mössinger, J. C., Allan, B. J., and Plane, J. M. C.: Active chlorine
999 release from marine aerosols: Roles for reactive iodine and nitrogen species, J. Geophys. Res,
1000 107, doi: 10.1029/2001JD000383, 2002.
1001
1002 Michalowski, B. A., Francisco, J. S., Li, S. M., Barrie, L. A., Bottenheim, J. W., and Shepson, P.
1003 B.: A computer model study of multiphase chemistry in the Arctic boundary layer during polar
1004 sunrise, J. Geophys. Res., 105, 15131 – 15145, 2000.
1005
1006 Mielke, L. H., Furgeson, A., and Osthoff, H. D.: Observation of $ClNO_2$ in a mid-continental
1007 urban environment, Environ. Sci. Technol., 45, 8889-8896, 2011.
1008
1009 Monks, P. S.: Gas-phase radical chemistry in the troposphere, Chem. Soc. Rev., 34, 376-395,
1010 2005.
1011
1012 Neuman, J. A., Nowak, J. B., Huey, L. G., Burkholder, J. B., Dibb, J. E., Holloway, J. S., Liao, J.,
1013 Peischl, J., Roberts, J. M., Ryerson, T. B., Scheuer, E., Stark, H., Stickel, R. E., Tanner, D. J.,
1014 and Weinheimer, A.: Bromine measurements in ozone depleted air over the Arctic Ocean, Atmos.
1015 Chem. Phys., 10, 6503-6514, 2010.

Oum, K., Lakin, M., DeHaan, D., Brauers, T., and Finlayson-Pitts, B.: Formation of molecular chlorine from the photolysis of ozone and aqueous sea-salt particles, Science, 279, 74, 1998a.

Oum, K., Lakin, M., and Finlayson-Pitts, B.: Bromine activation in the troposphere by the dark reaction of O_3 with seawater ice, Geophys. Res. Lett., 25, 3923-3926, 1998b.

Papanastasiou, D.K., McKeen, S. A., and Burkholder, J. B.: The very short-lived ozone depleting substance CHBr3 (bromoform): revised UV absorption spectrum, atmospheric lifetime, and ozone depletion potential, Atmos. Chem. Phys., 14, 3017 – 3025, 2014.

Piot, M., and Von Glasow, R.: The potential importance of frost flowers, recycling on snow, and open leads for ozone depletion events, Atmos. Chem. Phys., 8, 2437-2467, 2008.

Platt, U., and Janssen, C.: Observation and role of the free radicals NO_3, ClO, BrO and IO in the troposphere, Faraday Discuss., 100, 175-198, 1995.

Pöhler, D., Vogel, L., Frieß, U., and Platt, U.: Observation of halogen species in the Amundsen Gulf, Arctic, by active long-path differential optical absorption spectroscopy, Proceedings of the National Academy of Sciences, 107, 6582, 2010.

Pratt, K. A., Custard, K. D., Shepson, P. B., Douglas, T. A., Pöhler, D., General, S., Zielcke, J., Simpson, W. R., Platt, U., Tanner, D. J., Huey, L. G., Carlsen, M., and Stirm, B. H.: Photochemical production of molecular bromine in Arctic surface snowpacks, Nature Geosci., 6, 351 – 356, doi: 10.1038/ngeo1779, 2013.

Raso, A. R. W., Custard, K. D., Pratt, K. A., Tanner, D. J., Huey, L. G., and Shepson, P. B.: Active molecular iodine snowpack photochemistry in the Arctic, Proc. Nat. Acad. Sci., submitted, 2016.

Saiz-Lopez, A., Mahajan, A. S., Salmon, R. A., Bauguitte, S. J. B., Jones, A. E., Roscoe, H. K., and Plane, J. M. C.: Boundary layer halogens in coastal Antarctica, Science, 317, 348-351, 2007.

Saiz-Lopez, A., Plane, J. M. C., Mahajan, A. S., Anderson, P. S., Bauguitte, S. J. B., Jones, A. E., Roscoe, H. K., Salmon, R. A., Bloss, W. J., and Lee, J. D.: On the vertical distribution of boundary layer halogens over coastal Antarctica: implications for O_3, HO_x, NO_x and the Hg lifetime, Atmos. Chem. Phys., 8, 887-900, 2008.

Sander, R., Keene, W. C., Pszenny, A. A. P., Arimoto, R., Ayers, G. P., Baboukas, E., Cainey, J. M., Crutzen, P. J., Duce, R. A., Hönninger, G., Huebert, B. J., Maenhaut, W., Mihalopoulos, N., Turekian, C., and van Dingenen, R.: Inorganic bromine in the marine boundary layer: a critical review, Atmos. Chem. Phys., 3, 1301-1336, 2003.

Shetter, R. E., and Müller, M.: Photolysis frequency measurements using actinic flux spectroradiometry during the PEM-Tropics mission: Instrumentation description and some results, J. Geophys. Res., 104, 5647-5661, 1999.

Shepson, P. B., Sirju, A.-P., Hopper, J. F., Barrie, L. A., Young, V., Niki, H. and Dryfhout, H.: Sources and sinks of carbonyl compounds in the Arctic Ocean boundary layer: a polar ice floe experiment, J. Geophys. Res., 101, 21081 - 21089, 1996.

Staebler, R. M., den Hartog, G., Georgi, B., and Sterdiek, T. D.: Aerosol size distribution in Arctic haze during the Polar Sunrise Experiment 1992, J. Geophys. Res., 99, 25429-25437, 1994.

Sumner, A. L., and Shepson, P. B.: Snowpack production of formaldehyde and its effect on the Arctic troposphere, Nature, 398, 230-233, 1999.

Stephens, C. R., Shepson, P. B., Steffen, A., Bottenheim, J. W., Liao, J., Huey, L. G., Apel, E., Weinheimer, A., Hall, S. R., and Cantrell, C.: The relative importance of chlorine and bromine radicals in the oxidation of atmospheric mercury at Barrow, Alaska, J. Geophys. Res., 117, D00R11, doi: 10.1029/2011JD016649, 2012.

Sturges, W., and Barrie, L.: Chlorine, bromine and iodine in Arctic aerosols, Atmos. Environ., 22, 1179-1194, 1988.

Tang, T., and McConnell, J.: Autocatalytic release of bromine from Arctic snow pack during polar sunrise, Geophys. Res. Lett., 23, 2633-2636, 1996.

Thomas, J. L., Stutz, J., Lefer, B., Huey, L. G., Toyota, K., Dibb, J. E., and von Glasow, R.: Modeling chemistry in and above snow at Summit, Greenland – Part 1: Model description and results, Atmos. Chem. Phys., 11, 4899-4914, 2011.

Thompson, C. R., Shepson, P. B., Liao, J., Huey, L. G., Apel, E. C., Cantrell, C. A., Flocke, F., Orlando, J., Fried, A., Hall, S. R., Hornbrook, R. S., Knapp, D. J., Mauldin III, R. L., Montzka, D. D., Sive, B. C., Ullmann, K., Weibring, P. and Weinheimer, A.: Interactions of bromine, chlorine, and iodine photochemistry during ozone depletions in Barrow, Alaska, Atmos. Chem. Phys., 15, 9651 – 9679, doi: 10.5194/acp-15-9651-2015, 2015.

Thornton, J. A., Kercher, J. P., Riedel, T. P., Wagner, N. L., Cozic, J., Holloway, J. S., Dubé, W. P., Wolfe, G. M., Quinn, P. K., Middlebrook, A. M., Alexander, B., and Brown, S. S.: A large atomic chlorine source inferred from mid-continental reactive nitrogen chemistry, Nature, 464, 271-274, 2010.

Toyota, K., McConnell, J. C., Lupu, A., Neary, L., McLinden, C. A., Richter, A., Kwok, R., Semeniuk, K., Kaminski, J. W., Gong, S. –L., Jarosz, J., Chipperfield, M. P., and Sioris, C. E.: Analysis of reactive bromine production and ozone depletion in the Arctic boundary layer using 3-D simulations with GEM-AQ: inference from synoptic-scale patterns, Atmos. Chem. Phys., 11, 3949-3979, 2011.

Toyota, K., McConnell, J. C., Staebler, R. M., and Dastoor, A. P.: Air-snowpack exchange of bromine, ozone and mercury in the springtime Arctic simulated by the 1-D model PHANTAS -

Part 1: In-snow bromine activation and its impact on ozone, Atmos. Chem. Phys., 14, 4101-4133, 2014.

Vogt, R., Crutzen, P. J., and Sander, R.: A mechanism for halogen release from sea-salt aerosol in the remote marine boundary layer, Nature, 383, 327 – 330, doi: 10.1038/383327a0, 1996.

Vogt, R., Sander, R., von Glasow, R., and Crutzen, P. J.: Iodine chemistry and its role in halogen activation and ozone loss in the marine boundary layer: A model study, J. Atmos. Chem., 32, 375-395, 1999.

Wennberg, P., Hanisco, T., Jaegle, L., Jacob, D., Hintsa, E., Lanzendorf, E., Anderson, J., Gao, R. S., Keim, E., and Donnelly, S.: Hydrogen radicals, nitrogen radicals, and the production of O_3 in the upper troposphere, Science, 279, 49-53, 1998.

Young, C. J., Washenfelder, R. A., Roberts, J. M., Mielke, L. H., Osthoff, H. D., Tsai, C., Pikelnayai, O., Stutz, J., Veres, P. R., Cochran, A. K., VandenBoer, T. C., Flynn, J., Grossberg, N., Haman, C. L., Lefer, B., Stark, H., Graus, M., de Gouw, J., Gilman, J. B., Kuster, W. C., and Brown, S. S.: Vertically resolved measurements of nighttime radical reservoirs in Los Angeles and their contribution to the urban radical budget, Environ. Sci. Technol., 46, 10965-10973, 2012.

Zeng, T., Wang, Y., Chance, K., Blake, N., Blake, D., and Ridley, B.: Halogen-driven low-altitude O_3 and hydrocarbon losses in spring at northern high latitudes, J. Geophys. Res, 111, D17, doi: 10.1029/2005JD006706, 2006.

Table 1. Reactions used in the model that are pertinent to bromine chemistry. All rate constants (with the exception of photolysis *J* coefficients) are in units of cm^3 $molecule^{-1}$ s^{-1}.

Gas-Phase Reactions	**Rate Constant**	**Reference**
$Br + O_3 \rightarrow BrO$	6.75×10^{-13}	*Atkinson et al.* [2004]
$Br + C_2H_4 \rightarrow HBr + C_2H_5OO$	1.3×10^{-13}	*Atkinson et al.* [2004]
$Br + C_3H_6 \rightarrow HBr + C_3H_5$	1.60×10^{-12}	*Atkinson et al.* [2004]
$Br + HCHO \rightarrow HBr + CO + HO_2$	6.75×10^{-13}	*Sander et al.* [2006]
$Br + CH_3CHO \rightarrow HBr + CH_3COOO$	2.8×10^{-12}	*Atkinson et al.* [2004]
$Br + C_3H_6O \rightarrow HBr$	9.7×10^{-12}	*Wallington et al.* [1989]
Br + nButanal → HBr	9.7×10^{-12}	estimate from *Michalowski et al.* [2000]
$Br + CH_3OOH \rightarrow HBr + CH_3OO$	4.03×10^{-15}	*Mallard et al.* [1993]
$Br + NO_2 \rightarrow BrNO_2$	2.7×10^{-11}	*Atkinson et al.* [2004]
$Br + BrNO_3 \rightarrow Br_2 + NO_3$	4.9×10^{-11}	*Orlando and Tyndall* [1996]
$Br + OClO \rightarrow BrO + ClO$	1.43×10^{-13}	*Atkinson et al.* [2004]
$BrO + O(^3P) \rightarrow Br$	4.8×10^{-11}	*Atkinson et al.* [2004]
$BrO + OH \rightarrow Br + HO_2$	4.93×10^{-11}	*Atkinson et al.* [2004]
$BrO + HO_2 \rightarrow HOBr$	3.38×10^{-11}	*Atkinson et al.* [2004]
$BrO + CH_3OO \rightarrow HOBr + CH_2OO$	4.1×10^{-12}	*Aranda et al.* [1997]
$BrO + CH_3OO \rightarrow Br + HCHO + HO_2$	1.6×10^{-12}	*Aranda et al.* [1997]
$BrO + CH_3COOO \rightarrow Br + CH_3COO$	1.7×10^{-12}	estimate from *Michalowski et al.* [2000]
$BrO + C_3H_6O \rightarrow HOBr$	1.5×10^{-14}	estimate from *Michalowski et al.* [2000]
$BrO + NO \rightarrow Br + NO_2$	2.48×10^{-11}	*Atkinson et al.* [2004]
$BrO + NO_2 \rightarrow BrNO_3$	1.53×10^{-11}	*Atkinson et al.* [2004]
$BrO + BrO \rightarrow Br + Br$	2.82×10^{-12}	*Sander et al.* [2006]

$BrO + BrO \rightarrow Br_2$	9.3×10^{-13}		*Sander et al.* [2006]
$BrO + HBr \rightarrow HOBr + Br$	2.1×10^{-14}		*Hansen et al.* [1999]
$HBr + OH \rightarrow Br + H_2O$	1.26×10^{-11}		*Sander et al.* [2006]
$CH_3Br + OH \rightarrow H_2O + Br$	1.27×10^{-14}		*Atkinson et al.* [2004]
$CHBr_3 + OH \rightarrow H_2O + Br$	1.2×10^{-13}		*Atkinson et al.* [2004]
$Cl + BrCl \leftrightarrow Br + Cl_2$	f: 1.5×10^{-11}	r: 1.1×10^{-15}	*Clyne et al.* [1972]
$Cl + Br_2 \leftrightarrow BrCl + Br$	f: 1.2×10^{-10}	r: 3.3×10^{-15}	*Clyne et al.* [1972]
$BrO + ClO \rightarrow Br + Cl$	7.04×10^{-12}		*Atkinson et al.* [2004]
$BrO + ClO \rightarrow BrCl$	1.15×10^{-12}		*Atkinson et al.* [2004]
$BrO + ClO \rightarrow Br + OClO$	9.06×10^{-12}		*Atkinson et al.* [2004]
$HOBr + OH \rightarrow BrO + H_2O$	5.0×10^{-13}		*Kukui et al.* [1996]
$HOBr + Cl \rightarrow BrCl + OH$	8.0×10^{-11}		*Kukui et al.* [1996]
$HOBr + O(^3P) \rightarrow BrO + OH$	2.12×10^{-11}		*Atkinson et al.* [2004]
$IO + BrO \rightarrow Br + OIO$	9.36×10^{-11}		*Atkinson et al.* [2004]
$IO + BrO \rightarrow IBr$	4.32×10^{-11}		*Atkinson et al.* [2004]
$IO + BrO \rightarrow Br + I$	7.2×10^{-12}		*Atkinson et al.* [2004]

Photolysis Reactions	J_{max} **(25 March)** s^{-1}	**Lifetime**	**Reference**
$BrNO_3 \rightarrow Br + NO_3$	2.1×10^{-4}	1.3 h	calculated from OASIS data
$BrNO_3 \rightarrow BrO + NO_2$	1.2×10^{-3}	14.2 min	calculated from OASIS data
$BrO \rightarrow Br + O(^3P)$	3.0×10^{-2}	33 s	calculated from OASIS data
$Br_2 \rightarrow Br + Br$	4.4×10^{-2}	23 s	calculated from OASIS data
$HOBr \rightarrow Br + OH$	2.3×10^{-3}	7.2 min	calculated from OASIS data
$BrNO_2 \rightarrow Br + NO_2$	1.5×10^{-4}	1.8 h	estimate from *Lehrer et al.* [2004]
$BrCl \rightarrow Br + Cl$	1.26×10^{-2}	1.3 min	calculated from OASIS data

Mass Transfer Reactions	k_t **(forward)**	k_t **(reverse)**
$HBr_{(g)} \rightarrow H^+_{(p)} + Br^-_{(p)}$	1.80×10^{-3}	
$HCl_{(g)} \rightarrow H^+_{(p)} + Cl^-_{(p)}$	2.58×10^{-3}	
$HOBr_{(g)} \rightarrow HOBr_{(p)}$	1.26×10^{-3}	
$BrNO_{2(g)} \rightarrow BrNO_{2(p)}$	1.26×10^{-3}	
$BrONO_{3(g)} \rightarrow BrONO_{3(p)}$	1.26×10^{-3}	
$Br_{2(g)} \leftrightarrow Br_{2(p)}$	1.78×10^{-5}	2.97×10^{8}
$BrCl_{(g)} \leftrightarrow BrCl_{(p)}$	6.60×10^{-4}	1.91×10^{10}
$IBr_{(p)} \rightarrow IBr_{(g)}$	5.53×10^{9}	
$HBr_{(g)} \rightarrow H^+_{(s)} + Br^-_{(s)}$	1.67×10^{-5}	
$HCl_{(g)} \rightarrow H^+_{(s)} + Cl^-_{(s)}$	1.67×10^{-5}	
$HOBr_{(g)} \rightarrow HOBr_{(s)}$	1.67×10^{-5}	
$BrNO_{2(g)} \rightarrow BrNO_{2(s)}$	1.67×10^{-4}	
$BrONO_{3(g)} \rightarrow BrONO_{3(s)}$	1.26×10^{-4}	
$Br_{2(g)} \leftrightarrow Br_{2(s)}$	1.0×10^{-5}	7.71×10^{-2}
$BrCl_{(g)} \leftrightarrow BrCl_{(s)}$	1.25×10^{-5}	7.71×10^{-2}
$IBr_{(s)} \rightarrow IBr_{(g)}$	7.71×10^{-2}	

Aqueous Phase Reactions	k **(particle)**	k **(snow)**	**Reference**
$Cl^- + HOBr + H^+ \rightarrow BrCl$	5.17×10^{-21}	9.30×10^{-26}	*Wang et al.* [1994]
$Br^- + HOCl + H^+ \rightarrow BrCl$	1.2×10^{-24}	2.15×10^{-29}	*Sander et al.* [1997]
$Br^- + HOBr + H^+ \rightarrow Br_2$	1.47×10^{-20}	2.64×10^{-25}	*Beckwith et al.* [1996]
$Br^- + HOI + H^+ \rightarrow IBr$	3.04×10^{-18}	5.46×10^{-23}	*Troy et al.* [1991]
$BrCl + Cl^- \rightarrow BrCl_2^-$	3.3	5.99×10^{-5}	*Michalowski et al.* [2000]
$BrCl_2^- \rightarrow BrCl + Cl^-$	1.58×10^{9}	1.58×10^{9}	*Michalowski et al.* [2000]
$BrCl + Br^- \rightarrow Br_2Cl^-$	3.3	5.99×10^{-5}	*Michalowski et al.* [2000]
$Br_2Cl^- \rightarrow BrCl + Br^-$	3.34×10^{5}	3.34×10^{5}	*Wang et al.* [1994]
$Cl_2 + Br^- \rightarrow BrCl_2^-$	4.27	7.66×10^{-5}	*Wang et al.* [1994]
$BrCl_2^- \rightarrow Cl_2 + Br^-$	6.94×10^{2}	6.94×10^{2}	*Wang et al.* [1994]

$O_3 + Br^- \rightarrow HOBr$	4.5×10^{-9}	8.08×10^{-14}	*Oum et al.* [1998]

Table 2. Median mid-day bromine chain lengths for 25, 29, and 30 March 2009 (days with O_3 present) determined for four different modeling scenarios with different combinations of halogens present. Method 1 refers to Equation 3 (using terminations reactions) and Method 2 refers to Equation 4 (using initiation reactions).

	25 March		29 March		30 March		Average (1-σ st. deviation)	
	Method 1	Method 2	Method 1	Method 2	Method 1	Method 2	Method 1	Method 2
Br only	1.25	0.85	1.51	1.10	1.79	1.40	1.52 (± 0.27)	1.11 (± 0.28)
Br and Cl (Base)	1.29	0.84	1.43	1.03	1.58	1.29	1.43 (± 0.14)	1.05 (± 0.22)
Br and Low I	1.37	0.86	1.60	1.12	1.82	1.41	1.59 (± 0.22)	1.13 (± 0.28)
Br, Cl, and I	1.37	0.87	1.51	1.04	1.65	1.31	1.51 (± 0.14)	1.07 (± 0.23)

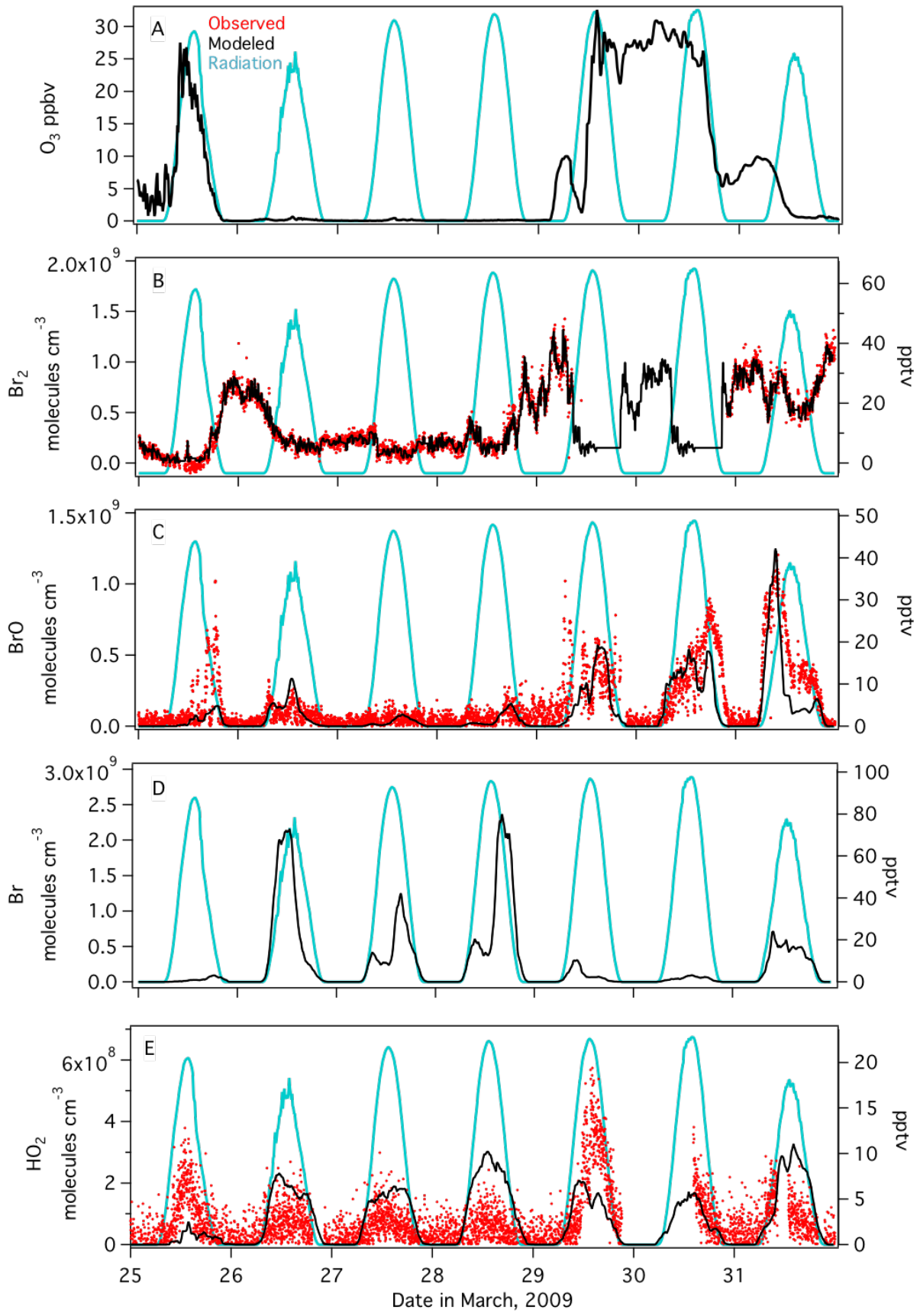
A
Observed
Modeled
Radiation
O_3 ppbv
B
Br_2 molecules cm^{-3}
ppt$v$
C
BrO molecules cm^{-3}
ppt$v$
D
Br molecules cm^{-3}
ppt$v$
E
HO_2 molecules cm^{-3}
ppt$v$
Date in March, 2009

1224

Fig 1. Time-series of gas-phase concentrations and mixing ratios of O_3, Br_2, BrO, Br, and HO_2 in the model (black trace) for the seven-day period simulated. Observations are plotted in red where available for Br_2, BrO, and HO_2. O_3 and Br_2 are constrained species in the model. Simulated output of BrO, Br, and HO_2 are smoothed by hourly averaging. Radiation is shown as the cyan trace as a reference. Time is expressed in Alaska Standard Time.

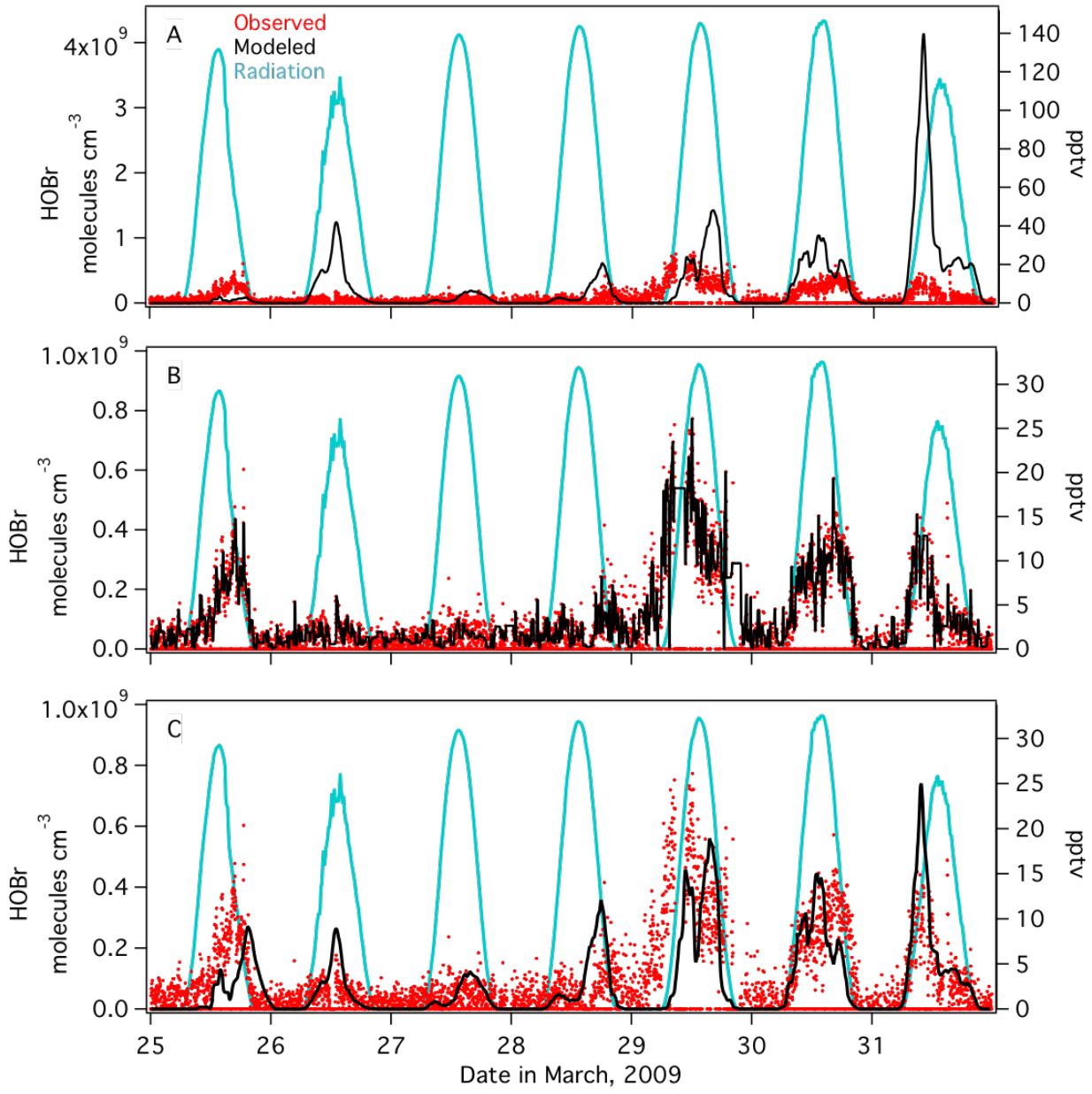

Fig 2. Simulated (black trace) versus observed (red markers) HOBr mixing ratios shown for three different versions of the model: A) HOBr unconstrained and allowed to freely evolve with a constant surface deposition term as described in the Methods, B) HOBr constrained to observations, C) HOBr unconstrained but with a variable surface deposition that is enhanced during higher wind speeds. Simulated (unconstrained) output in Panels A and C are smoothed by

hourly averaging. Radiation is shown as the cyan trace as a reference. Time is expressed in Alaska Standard Time.

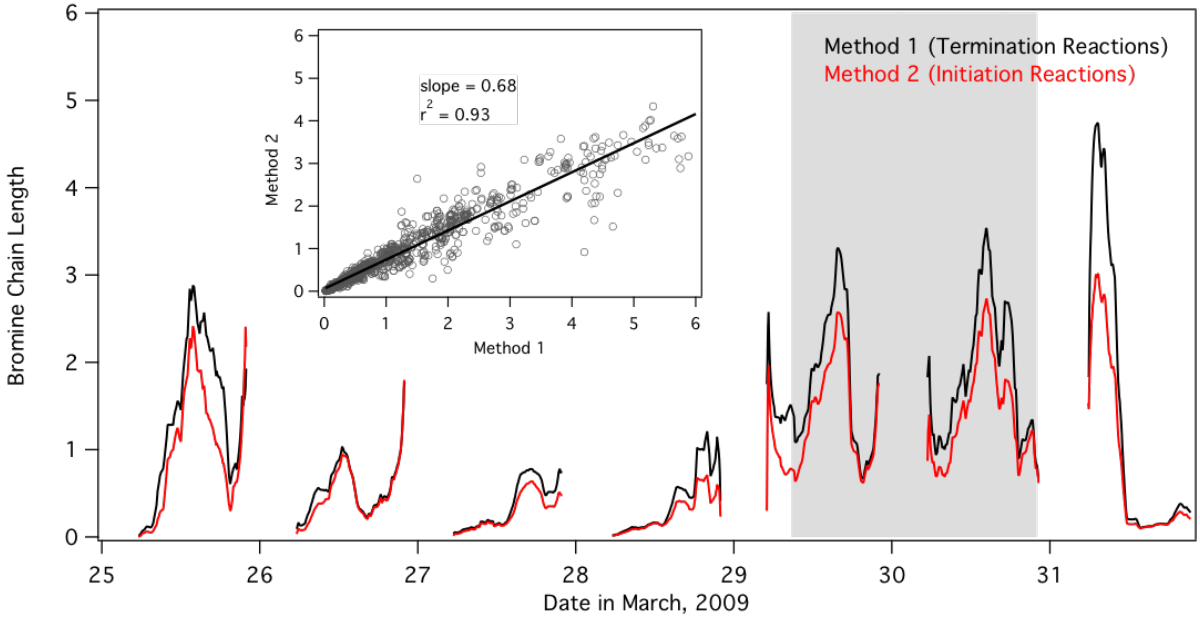

Fig 3. Time-series of model calculated bromine chain length for the daytime hours (7:00 to 21:00 AKST). Method 1 is plotted as the black trace and Method 2 is plotted as the red trace. Model output is smoothed by hourly averaging. The grey shaded box represents a period of missing Br_2 observations. The inset graph shows a linear regression of Method 1 and Method 2 calculations. Time is expressed in Alaska Standard Time.

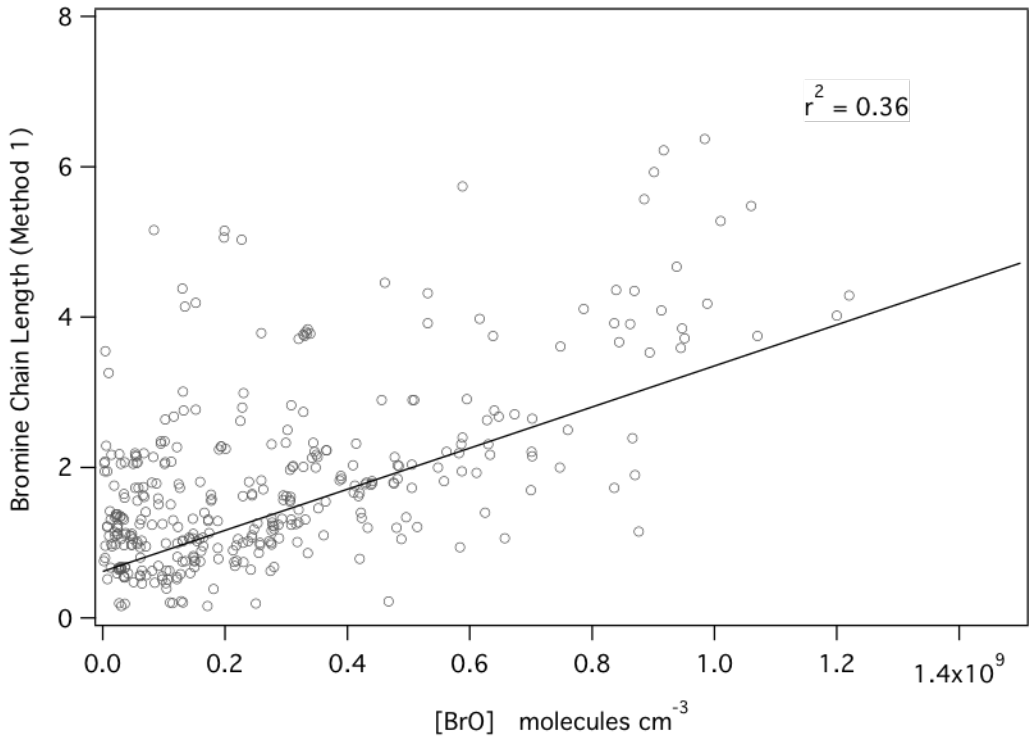

Fig 4. Regression of daytime (7:00 – 21:00 AKST) bromine chain length calculated by Method 1 (Equation 5) and simulated BrO concentration.

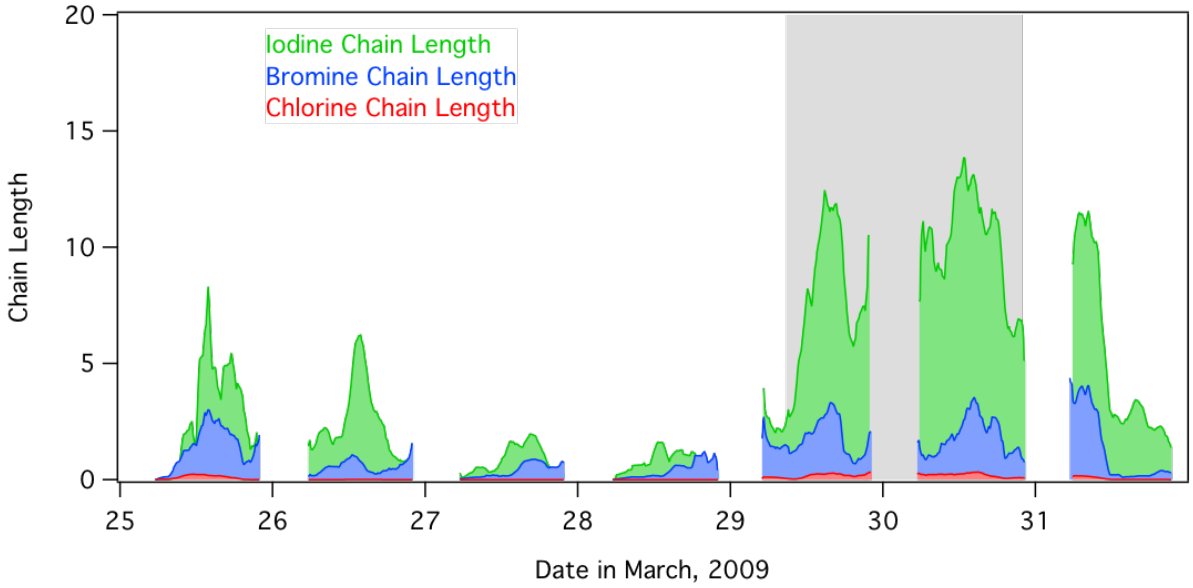

Fig 5. Calculated chain lengths for iodine (green), bromine (blue), and chlorine (red) across the seven days of the simulated period modeled using the Base + Iodine scenario. Model output is smoothed by hourly averaging. The grey shaded box represents a period of missing Br_2 observations. Time is expressed in Alaska Standard Time.

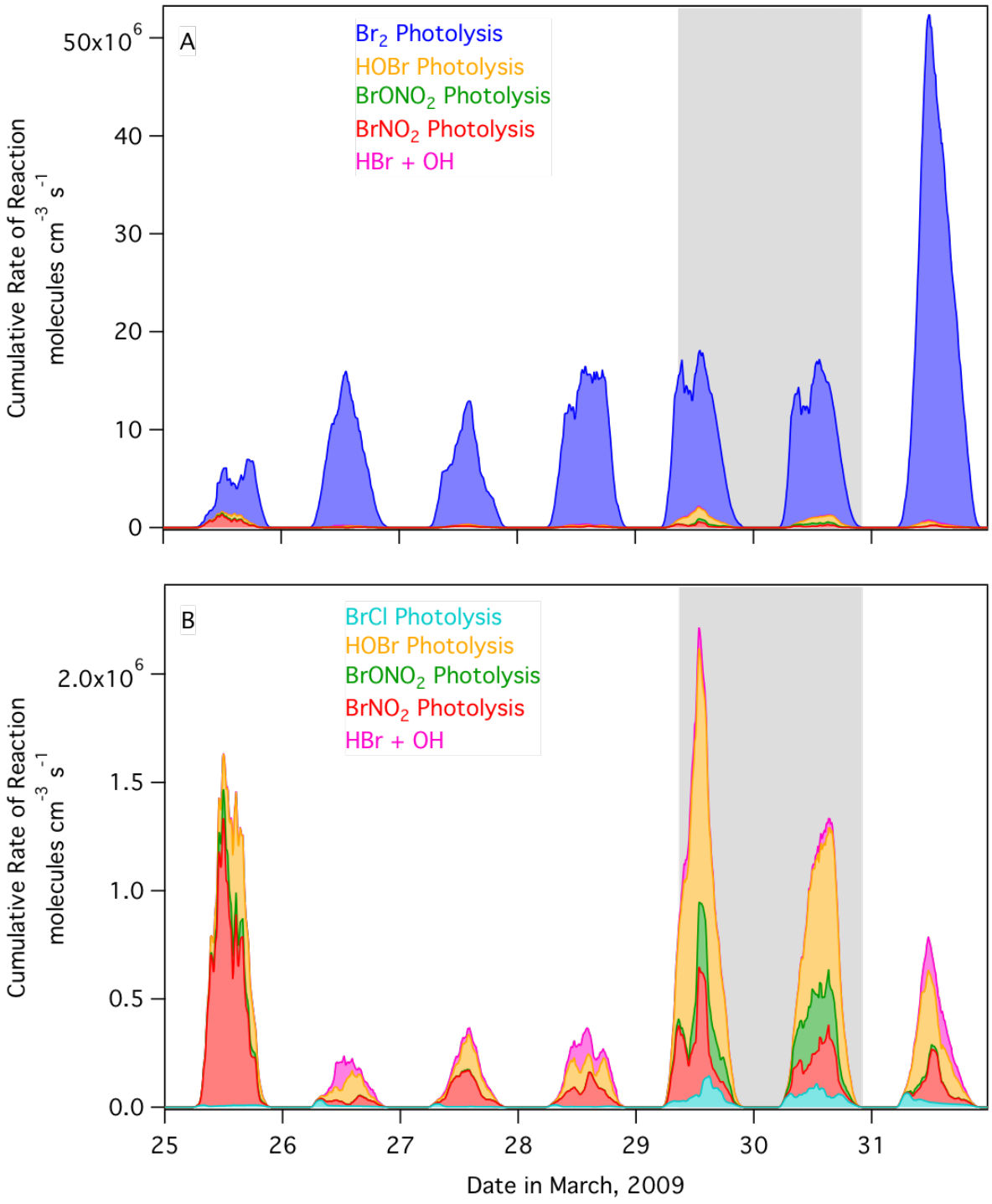

Fig 6. Time-varying rates of the most important bromine initiation reactions in the Base Model. Panel A includes photolysis of Br_2, which dominates the bromine initiation. Br_2 photolysis is calculated as 2 x $J_{Br2}[Br_2]$. In Panel B, Br_2 photolysis has been removed so that the minor terms can be visualized. Panel B also includes BrCl, which contributes only a negligible amount to

bromine initiation. Model output is smoothed by hourly averaging. The y-axis is expressed as a cumulative rate of reaction. The grey shaded box represents a period of missing Br_2 observations. Time is expressed in Alaska Standard Time.

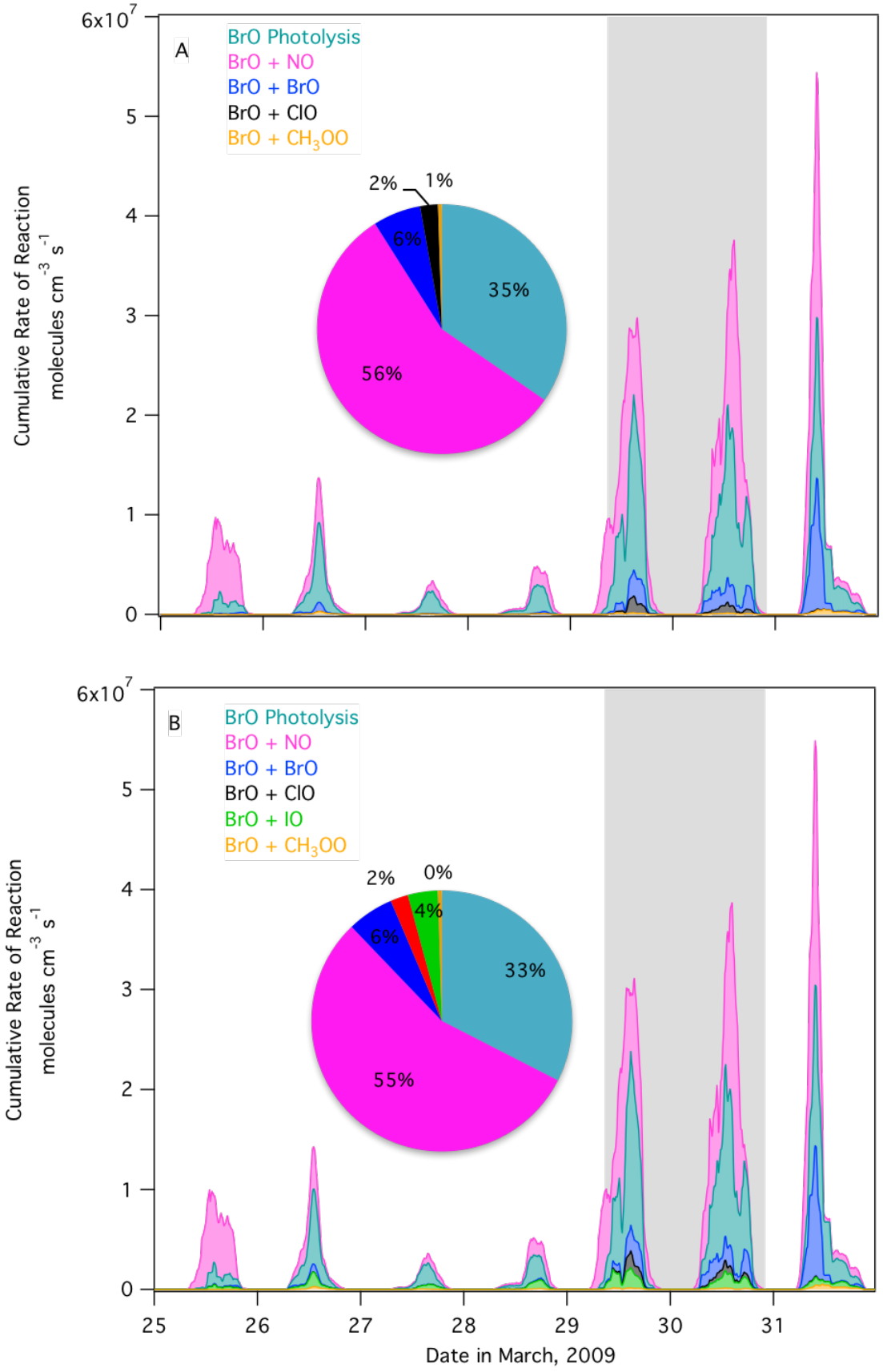
A
BrO Photolysis
BrO + NO
BrO + BrO
BrO + ClO
BrO + CH3OO
2%
1%
6%
35%
56%
6x10^7
5
4
3
2
1
0
Cumulative Rate of Reaction
molecules cm^-3 s^-1
B
BrO Photolysis
BrO + NO
BrO + BrO
BrO + ClO
BrO + IO
BrO + CH3OO
2%
0%
4%
6%
33%
55%
25
26
27
28
29
30
31
Date in March, 2009

1269

Fig 7. Time-varying rates of the most important bromine propagation reactions in the Base Model with Br and Cl present (Panel A) and with iodine included (Panel B). The BrO + BrO reaction is calculated as $2k[BrO]^2$ as this reaction regenerates two Br atoms. Model output is smoothed by hourly averaging. The y-axis is expressed as a cumulative rate of reaction. The grey shaded box represents a period of missing Br_2 observations. Time is expressed in Alaska Standard Time. The inset pie charts show the average fractional importance of each reaction pathway for only days 29 and 30 March (i.e. background O_3 days).

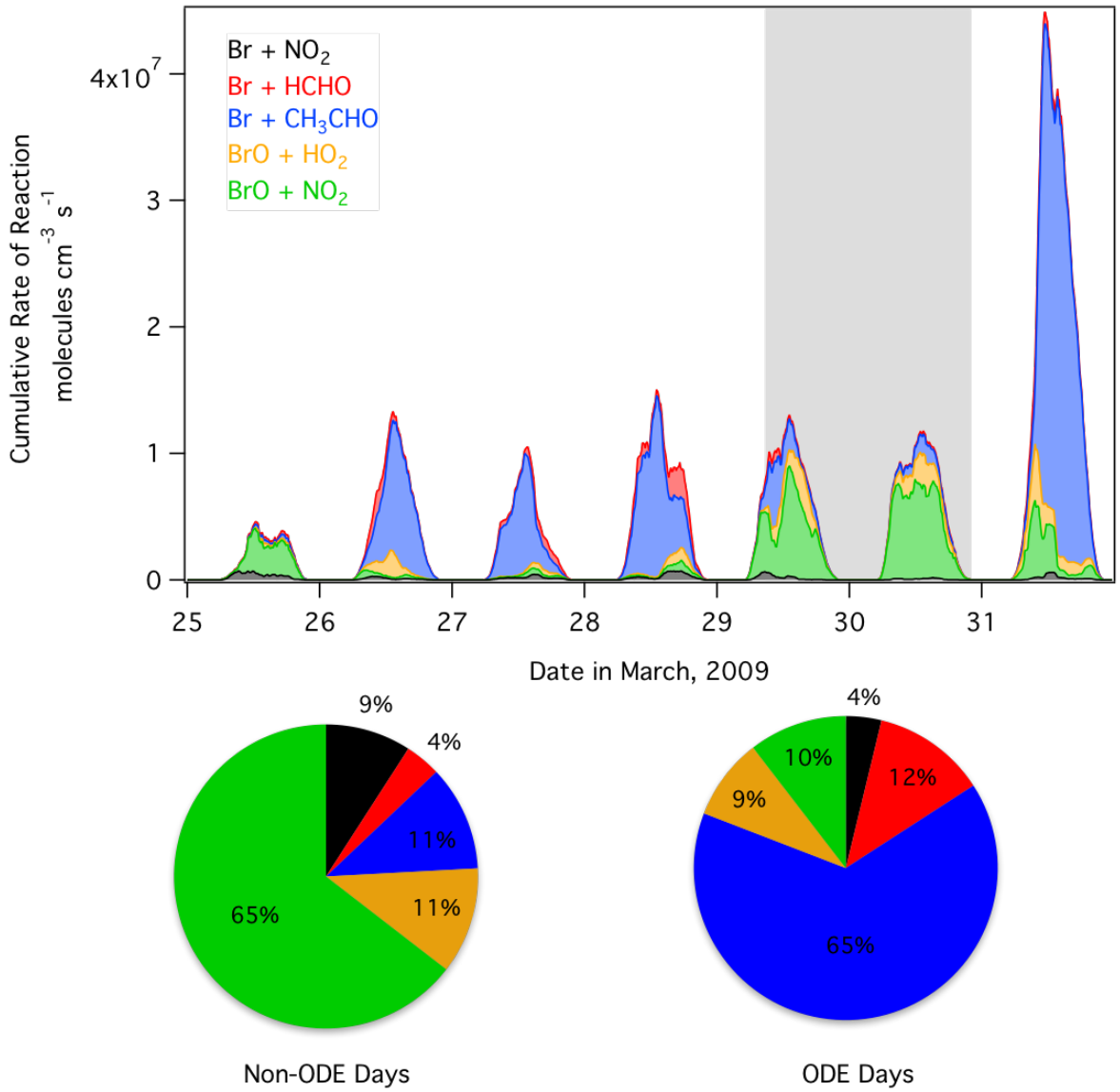

Fig 8. Time-varying rates of the most important reactive bromine (BrO_x) termination reactions in the Base Model. Model output is smoothed by hourly averaging. The y-axis is expressed as a cumulative rate of reaction. The grey shaded box represents a period of missing Br_2 observations. Time is expressed in Alaska Standard Time. The pie charts show the average fractional importance of each reactive bromine sink for non-ODE (background O_3) days and ODE days.

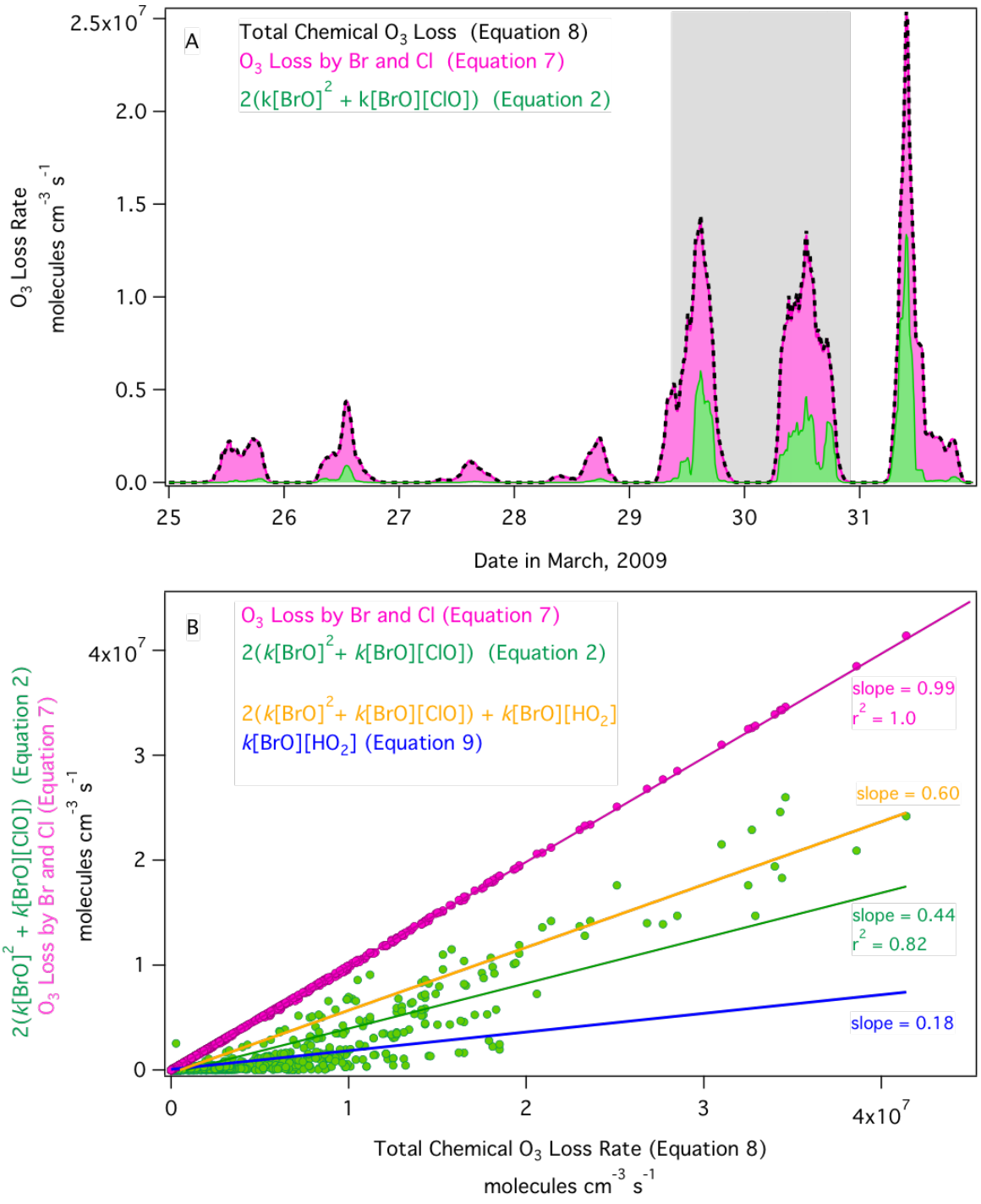

Fig 9. A) Comparison of the time-varying O_3 loss rate calculated using the estimation of $2(k[BrO]^2 + k[BrO][ClO])$ (Equation 2, green), the simulated O_3 loss rate by Br and Cl (Equation 7, pink), and the total simulated chemical O_3 loss rate (Equation 8, dashed black trace). Model output is smoothed by hourly averaging. The grey shaded box represents a period of missing Br_2 observations. Time is expressed in Alaska Standard Time. B) Shown is a regression of the

1291 $2(k[BrO]^2 + [BrO][ClO])$ estimation method (Equation 2) versus the total simulated chemical O_3
1292 loss rate in the Base Model (Equation 8) in the green data, and a regression of O_3 loss rate by Br
1293 and Cl only (Equation 7) versus the total simulated chemical O_3 loss rate in the pink data. The
1294 blue trace represents the O_3 loss rate estimated by only considering $k[BrO][HO_2]$ (Equation 9).
1295 The orange trace estimates O_3 loss rate combining the three major gas-phase ozone depletion
1296 cycles. The slopes represent the fraction of the chemical O_3 loss rate that can be accounted for by
1297 each method. For the conditions simulated, the commonly used estimation method of $2(k[BrO]^2$
1298 $+ [BrO][ClO])$ only accounts for 44% of the chemical O_3 loss rate.

1299

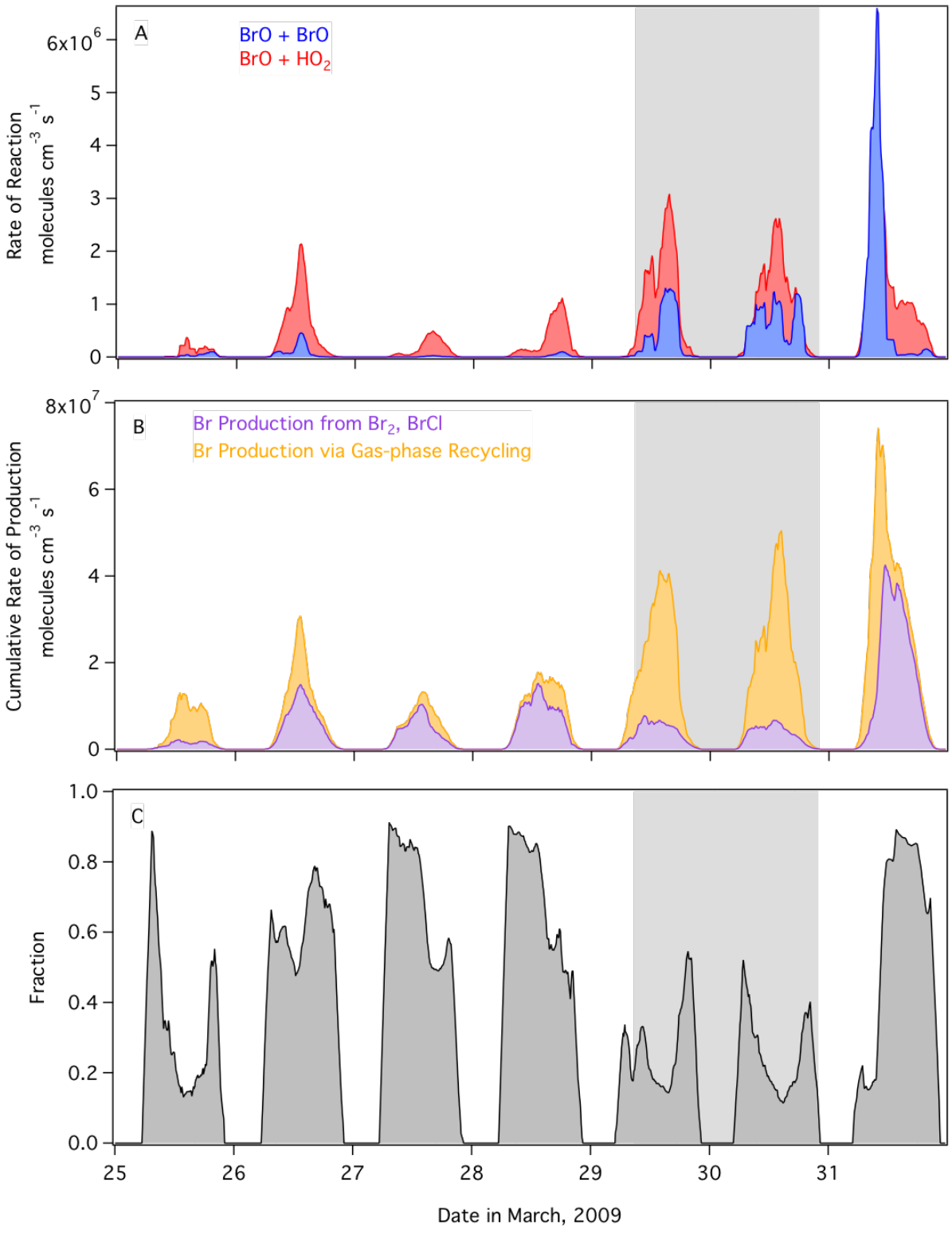

1300

1301 **Fig 10.** Panel A: Comparison of the rate of reaction of BrO + BrO (blue) and BrO + HO_2 (red).
1302 Panel B: The cumulative rate of Br atom production separated into the Br production rate from
1303 the photolysis of Br_2 and BrCl surface emissions calculated from Equation 10 (purple) and the Br

atom production rate due to gas-phase radical recycling calculated from Equation 11 (orange). Panel C: The fraction of total Br atom production due to production from Br_2 and BrCl surface emissions. In all panels, model output is smoothed by hourly averaging. The grey shaded box represents a period of missing Br_2 observations. Time is expressed in Alaska Standard Time.